Geophys. J. Int. (2003) **155,** 149–173

Seismotectonics of the Sinai subplate – the eastern Mediterranean region

Amos Salamon,[1] Avraham Hofstetter,[2] Zvi Garfunkel[3] and Hagai Ron[2,3]

[1] *The Geological Survey,* 30 *Malkhe Israel St., Jerusalem* 95501, *Israel. E-mail: salamon@mail.gsi.gov.il*
[2] *The Geophysical Institute of Israel,* PO Box 182, *Lod,* 71100, *Israel*
[3] *Department of Geology, The Hebrew University, Jerusalem,* 91904, *Israel*

Accepted 2003 April 29. Received 2003 April 17; in original form 2002 July 16

SUMMARY

We define the Sinai subplate, from a seismotectonic perspective, as a distinct component in the plate tectonics of the eastern Mediterranean region. This is based on the tectonic characteristics of a comprehensive listing of all $M_L \geq 4$ recorded seismicity in the region during the 20th century, on newly calculated and recalculated fault plane mechanisms of first *P*-wave arrivals and on published solutions based on waveform inversion of broad-band data.

The low seismicity level and scarcity of strong events in the region required a thorough search for useful data and a careful examination of the reliability of the focal solutions. We gathered all available records of first *P*-wave onsets from the ISS and ISC Bulletins and the local seismic networks. Altogether, we were able to calculate 48 new focal mechanisms and 33 recalculated ones of events that occurred during the years 1940–1992. With the increasing number of teleseismic and regional broad-band stations in the later years, we added 37 solutions based on teleseismic and regional waveform inversions of events that occurred during 1977–2001.

These mechanisms enabled us to examine the seismotectonic character of the Sinai subplate. The strike and rake directions of the calculated mechanisms usually reflect the geometry and the large-scale type of deformation observed along the boundaries of the Sinai subplate—the Dead Sea Transform, the Cypriot Arc convergent zone and the Suez Rift. Nevertheless, along each of these boundaries we found anomalous solutions that attest to the complexity of the deformation processes along plate margins.

Earthquakes along the Dead Sea Transform exhibit mainly sinistral transtension and transpression, reflecting its leaky manner and local change in the transform geometry. The presence of other unexpected mechanisms near the transform, however, reflects the heterogeneous deformation it induces around.

As expected, thrust mechanisms along the Cypriot Arc mirror its convergent nature and typical curved geometry. Transtension and transpressional solutions in the eastern segment of the arc reflect the sinistral shear motion between Anatolia and Sinai there. However, shear mechanisms found between Cyprus and the Eratosthenes Seamount pose a problem regarding its collision process.

Most intriguing of all are $M_L \geq 4$ thrust and shear solutions found in the Gulf of Suez. They are associated with predominantly normal mechanisms within a rift zone and therefore constitute a unique phenomenon, yet to be deciphered.

Key words: Cypriot Arc, Dead Sea Transform, earthquakes, fault-plane solutions, seismotectonics, Suez Rift.

1 INTRODUCTION

Seismotectonics is an advantageous tool in deciphering the neotectonics of seismogenic structures, especially along plate margins. Here we focus on the eastern Mediterranean region (Fig. 1), where the small Sinai subplate at the northeastern tip of the African Plate takes the major role in the local plate tectonics.

The Sinai subplate is situated at the juncture of the African, Arabian and Anatolian plates (McKenzie 1970; McKenzie *et al.* 1970; Ben-Menahem *et al.* 1976; Le Pichon & Francheteau 1978; Joffe

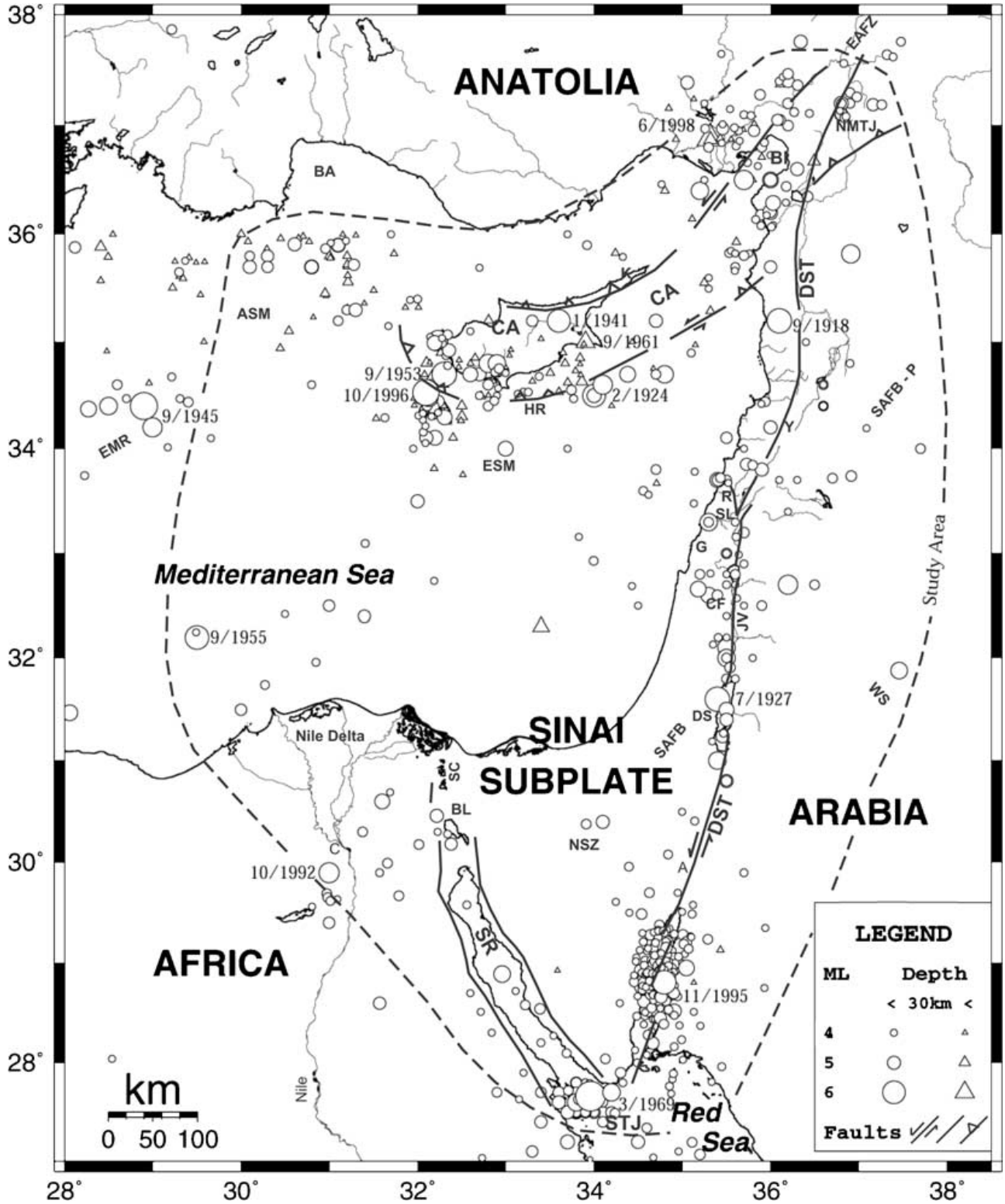

Figure 1. Seismicity and tectonics of the study area (modified after Garfunkel *et al.* 1981; Kempler & Garfunkel 1991; Salamon *et al.* 1996). Most of the $M_L \geq 5$ events are concentrated along the plate borders while the smaller events are scattered around. The plates are: Africa, Arabia, Anatolia and the Sinai subplate. The plate borders are: Cypriot Arc (CA), Dead Sea Transform (DST) and Suez Rift (SR). Other geological elements and localities: A, Arava Valley; ASM, Anaximander Seamount; BA, Bay of Antalya; BI, Bay of Iskenderun; BL, Bitter Lakes; C, Cairo; CF, Carmel–Faria fault system; DS, Dead Sea; EAFZ, East Anatolian Fracture Zone; EMR, East Mediterranean Ridge; ESM, Eratosthenes Seamount; G, Galilee; GA, Gulf of Aqaba; HR, Hecteaus Rise; JV, Jordan Valley; K, Kyrenia; NMTJ, Northeast Mediterranean Triple Junction; NSZ, Negev Shear Zone; P, Palmyrides; R, Roum fault; SAFB, Syrian Arc Fold Belt (including P, Palmyrides); SC, Suez Canal; SL, South Lebanon; STJ, Sinai Triple Junction; WS, Wadi Sirhan; Y, Yammouneh bend.

& Garfunkel 1987). It includes a portion of the Eastern Mediterranean and the Levant Basin. These regions have been shaped since the Early Mesozoic by a series of rifting phases that formed the northeastern margin of the once continuous Afro-Arabian continent (Garfunkel & Derin 1985; Ben-Avraham & Ginzburg 1990; Garfunkel 1998). The Sinai subplate is a new tectonic element that was formed as a result of a Cenozoic breakup of the Eastern Mediterranean and the Levant Basin. Many researchers studied the geology, tectonic style and kinematics of its borders: the Dead Sea left-lateral Transform (DST), which accommodates the motion between Arabia and Sinai (northeastern tip of Africa) (Freund 1965; Wilson 1965; Freund *et al.* 1970; Ben-Menahem *et al.* 1976; Garfunkel 1981); the convergent Cypriot Arc (CA) at the suture between Anatolia and Sinai (McKenzie 1970, 1972; Dewey *et al.* 1973; Woodside 1977; Rotstein & Kafka 1982; Kempler & Ben-Avraham 1987; Kempler & Garfunkel 1991); and the Suez Rift (SR), which carries some divergence motion between Africa and Sinai (Garfunkel & Bartov 1977; Patton *et al.* 1994; Bosworth & McClay 2001). While clearly these are plate boundaries, there is almost no morphologic (Hall 1994), tectonic (Garfunkel & Bartov 1977) or seismic (Salamon *et al.* 1996) evidence of a northward continuation of the SR toward the CA, to completely encircle Sinai and define it as a microplate. Bosworth & McClay (2001), however, partly continue the SR northward, via a regional left-stepping relay beneath the Nile Delta. Recently, Mascle *et al.* (2000) identified an active fault belt that might correspond to an offshore extension of the SR, and suggested that this belt represents the western border of the Sinai subplate. However, its right lateral sense of motion is still a matter of debate.

In the first seismotectonic analysis of the area, Ben-Menahem *et al.* (1976) described the regional plate tectonic elements in light of their seismicity and concluded that: 'The Sinai region should not be considered a separate plate, but rather a splinter of the Africa plate, which is breaking up incoherently as it approaches the zone of collision.' The other seismotectonic studies focused on particular events or fault segments, either along plate borders or intraplate structures. Note these are studies of the strongest events along the Sinai borders. They occurred in the Gulf of Aqaba (Elat) in 1995 November ($M_L = 6.2$; $M_W = 7.2$; e.g. Shamir *et al.* 2003; Pinar & Turkelli 1997; Klinger *et al.* 1999), and in Shadwan in 1969 March ($M_L = 6.6$; e.g. Ben-Menahem & Aboodi 1971; Jackson *et al.* 1988). These events reflect the sinisteral motion along the DST and the extension in the SR, respectively. Left-lateral mechanisms found both in moderate events (Ben-Menahem *et al.* 1976; Arieh *et al.* 1982) and in microseismicity (van Eck & Hofstetter 1989) characterize faulting in the Dead Sea basin, and the Jordan Valley (van Eck & Hofstetter 1990). The intraplate Carmel-Fari'a tectonic system, which releases some of the seismicity off the Sinai subplate boundaries, was found to have a sinistral transpressional motion (Hofstetter *et al.* 1996; Ron *et al.* 1990). Other mechanisms, including small events, were also published in the IPRG (Institute for Petroleum Research and Geophysics) Bulletins (1982–1993), Kovach *et al.* (1990), Badawy & Horvath (1999), Badawy (2001), Badawy & Abdel Fattah (2001), Hurukawa *et al.* (2001), and catalogued by Udias *et al.* (1989, and references therein).

These important works outline the characteristics of the Sinai subplate borders. However, our recent comprehensive list of earthquakes that covers a century-long time span (Salamon 1993), revealed many data that were not used until now. It showed the low to moderate level of seismicity within the Sinai subplate and the concentration of the $M_L \geq 5$ events within a seismogenic belt along the subplate boundaries (Salamon *et al.* 1996). Moreover, it enabled us to calculate 48 new focal mechanisms and recalculate another 33 solutions of $M_L \geq 4$ events, based on the polarity of first *P*-wave arrivals (Table 1 and Appendix A). With the increasing number of teleseismic and regional broad-band stations during recent years, we tend to use solutions based on waveform inversion of broad-band data rather than the mechanisms obtained by the use of first-motion *P*-wave onsets. Therefore, we accept the former solutions, with no change on our part, and use them in the discussion of the tectonic interpretation (Table 2).

Using our 81 new and recalculated mechanisms based on *P*-wave onsets together with 37 additional solutions based on broad-band data, we were able to prepare a more comprehensive seismotectonic picture of the Sinai subplate than was possible earlier. This enabled us to examine, on the one hand, the nature of the ongoing principal deformation along the subplate borders with relation to the plate motions; and on the other hand, we were able to evaluate the complexity of the secondary deformation along the subplate borders and within it.

2 FAULT PLANE SOLUTIONS

2.1 Focal solutions based on first *P*-wave arrivals

2.1.1 Sources of data

Following the comprehensive list of Salamon (1993), we systematically searched the available seismological records and literature for readings of first *P*-wave arrivals in order to calculate new focal plane solutions. These sources include the bulletins of the international organizations ISS and ISC, NEIC, the national bulletins of Israel (IPRG 1982–1993; GII 1996) and Jordan (JSO 1984–1993) and the seismograms of the WWSSN deployed in the region: EIL, HLW and JER.

2.1.2 Program and calculations

To calculate the focal solutions we used the program FPFIT and FPPLOT (Reasenberg & Oppenheimer 1985). Incident angles of first *P*-wave arrivals to stations with distances greater than 2° from the epicentre are given in the tables of Pho & Behe (1972). Incident angles to stations closer than 2° to the epicentre were calculated according to the crustal velocity model in use by the IPRG for routine data processing (3.5, 5.7 and 6.4 km s^{-1} for thickness intervals of 2.1, 10.6 and 15.5 km, respectively; and 7.9 km s^{-1} for depth ≥28.2 km; IPRG Bulletins). Since the control on the hypocentral depth determination in most cases was poor, we arbitrarily set it to 10 km. Changes in the hypocentral depth or in the velocity model have a negligible effect on the incident angles of far (>2°) *P*-wave arrivals (van Eck & Hofstetter 1990), which most of the solutions are based on. Where relevant, i.e. where the solutions contain many readings of near stations, we examined its stability in relation to changes of depth.

2.1.3 Quality of data and reliability of solutions

The low seismicity and the insufficient coverage of seismographic stations until the 1980s limit the number of fault plane solutions that can be obtained in the region. We therefore carefully examined the available data and the reliability of the solutions in order to get the most out of them. In our case, only 75 out of approximately

Table 1. Parameters of the fault plane solutions of first *P*-wave arrivals, calculated in this study by the FPFIT program (Reasenberg & Oppenheimer 1985). All are $M_L \geq 4$ events that occurred within the eastern Mediterranean region, during the years 1940–1992, for which we found sufficient data.

Event								Parameters of fault plane solutions									
								P		*T*		First plane			Second plane		
No	Symbol	Origin time		M_L	Lat.	Long.	Zone	ϕ	δ	ϕ	δ	ϕ	δ	L	ϕ	δ	L
1	8/40a	1940	08161602	5.1	35.7	30.8	CA	7	255	20	348	70	120	170	80	213	20
2	8/40b	1940	08161823	5.0	35.7	30.8	CA	11	67	52	322	65	95	130	46	211	35
3	1/41	1941	01200337	6.0	35.2	33.6	CA	11	122	52	227	46	338	144	65	95	50
4*	9/45	1945	09021154	6.4	34.4	28.9	Med	10	337	78	186	35	150	80	55	342	96
5	4/51	1951	04082138	5.7	36.5	35.7	CA	66	41	17	263	30	105	−60	64	251	−106
6	9/53	1953	09100406	6.2	34.7	32.3	CA	2	271	24	3	75	230	20	70	134	64
7	9/55	1955	09120609	6.1	32.2	29.5	Med	19	305	70	125	25	125	90	65	305	90
8	3/56a	1956	03161932	5.2	33.3	35.3	DST	10	144	10	235	90	280	−15	75	10	−180
9	3/56b	1956	03161943	5.5	33.3	35.3	DST	18	155	34	51	50	288	12	80	190	140
10	12/56	1956	12181753	5.2	31.5	35.5	DST	57	39	22	269	71	251	−113	30	125	−40
11*	6/59	1959	06131201	5.5	34.8	32.9	CA	5	2	81	132	40	190	100	50	357	81
12	9/61	1961	09150146	6.0	35	33.9	CA	1	350	75	87	45	185	110	48	337	71
13	9/63	1963	09120818	5.0	34.8	32.1	CA	3	299	68	39	52	280	63	45	140	120
14*	1/65	1965	01251218	4.7	34.6	32.8	CA	1	350	75	87	45	185	110	48	337	71
15	4/66	1966	04081346	4.8	35.8	31	CA	9	101	31	5	75	140	150	61	238	17
16*	4/67a	1967	04071707	4.8	37.4	36.2	NMTJ	21	224	6	131	70	356	−10	80	90	−160
17*	4/67b	1967	04071833	4.9	37.4	36.2	NMTJ	6	16	21	109	80	335	20	70	241	169
18	6/67	1967	06151456	4.6	34.1	32.4	CA	31	50	9	146	75	185	−30	61	283	−162
19	3/68	1968	03261937	4.8	34.1	35.5	DST	27	251	0	341	70	120	−60	71	22	−21
20	11/68	1968	11061341	4.8	35.2	32.8	CA	3	329	68	69	45	170	120	52	310	63
21*	3/69a	1969	03241154	5.0	27.5	33.8	SR	8	335	69	92	40	180	120	56	322	67
22*	3/69b	1969	03241250	4.8	27.6	33.8	SR	55	228	32	27	78	35	−80	15	175	−130
23*	3/69c	1969	03270615	4.7	27.5	33.9	SR	10	271	55	16	45	125	140	62	245	52
24	3/69d	1969	03310716	6.6	27.66	33.96	SR	75	317	1	54	45	220	−110	48	67	−71
25	3/69e	1969	03312144	4.9	27.5	34	SR	22	254	57	24	30	110	140	71	236	66
26	4/69a	1969	04041218	4.7	27.7	34.1	SR	58	245	28	93	74	83	−103	20	305	−50
27	4/69b	1969	04081031	5.0	27.5	33.7	SR	25	250	65	69	70	250	−20	20	70	90
28	4/69c	1969	04231337	4.9	27.6	33.9	SR	24	120	10	215	80	255	−25	65	350	−170
29	5/69	1969	05100927	4.8	27.5	34.2	SR	71	320	7	75	39	237	−116	55	90	−70
30*	12/69	1969	12300510	4.8	27.5	33.9	SR	70	135	19	314	25	135	−90	65	315	−90
31	4/70	1970	04280320	4.8	27.7	33.6	SR	13	108	13	201	90	65	20	70	335	180
32*	7/70	1970	07011550	4.8	35.3	31.2	CA	16	55	70	202	30	150	110	61	47	78
33	10/70	1970	10051453	4.8	35.1	38.9	Plm	9	309	80	130	35	130	90	55	310	90
34	12/70	1970	12192244	4.6	27.5	33.9	SR	54	249	35	62	80	65	−86	10	225	−110
35	4/71	1971	04162127	4.6	33.7	35.5	DST	38	113	14	215	75	250	−40	51	352	−160
36	6/71	1971	06290908	5.0	37.1	36.8	NMTJ	11	312	62	65	40	160	130	60	292	61
37	7/71a	1971	07082340	5.1	27.2	33.7	SR	69	139	20	332	25	160	−80	65	328	−94
38	7/71b	1971	07112012	5.1	37.2	36.8	NMTJ	30	134	60	314	75	135	90	15	315	90
39	8/71	1971	08170429	4.9	37.1	36.8	NMTJ	32	132	55	333	78	140	99	15	280	50
40	1/72	1972	01120815	5.0	27.5	33.7	SR	66	91	17	313	30	155	−60	64	301	−106
41	6/72	1972	06280949	5.5	27.6	33.8	SR	62	335	19	108	30	260	−130	67	124	−69
42*	4/74	1974	04292005	5.2	30.6	31.6	Egp	27	252	27	147	90	110	−142	50	20	0
43*	1/75a	1975	01010030	5.2	36.67	36.49	NMTJ	55	316	30	103	77	116	−74	20	245	−140
44	1/75b	1975	01282112	4.6	34.71	33.5	CA	21	39	67	196	25	235	110	66	33	80
45	1/76a	1976	01121750	5.0	34.3	32.5	CA	27	131	0	221	70	0	−160	71	262	−21
46	1/76b	1976	01122019	4.9	34.4	32.5	CA	27	108	14	205	60	340	−170	81	244	−30
47	1/76c	1976	01262244	4.6	35.8	31.2	CA	63	202	25	5	20	170	−110	71	11	−82
48	2/78	1978	02092110	4.5	37.07	36.84	NMTJ	17	11	66	233	30	170	60	64	23	106
49	4/79a	1979	04042117	4.4	35.96	30.65	CA	57	194	31	30	15	235	−60	77	24	−97
50	4/79b	1979	04231301	5.0	31.24	35.46	DST	3	320	17	51	80	277	15	75	185	170
51*	9/79	1979	09201037	4.0	35.23	30.82	CA	34	39	55	220	10	220	90	80	40	90
52	1/80	1980	01021252	4.7	36.6	36.4	NMTJ	30	1	55	148	77	348	74	20	220	140
53	2/81	1981	02190241	4.7	36.35	36.42	DST	3	49	10	139	85	5	10	80	274	174
54	6/81	1981	06300759	4.7	36.18	35.89	DST	21	201	33	306	82	166	40	50	70	170
55	8/81	1981	08100521	4.6	36	30	CA	0	255	67	347	50	235	60	48	96	120
56*	3/82	1982	03231048	4.7	27.9	34.3	Elt	45	90	6	186	65	220	−40	54	329	−148
57	5/82	1982	05200328	4.6	34.62	33.7	CA	1	5	75	102	45	200	70	48	352	71
58	6/83a	1983	06030204	4.9	33.85	35.73	DST	65	77	5	179	55	200	−60	44	344	−125
59	6/83b	1983	06121200	5.4	28.89	32.96	SR	0	74	67	342	50	95	120	48	233	59
60	9/83	1983	09241640	4.6	34.53	33.6	CA	27	141	0	231	70	10	−160	71	272	−21

Table 1. (*Continued.*)

Event								Parameters of fault plane solutions									
								P		*T*		First plane			Second plane		
No	Symbol	Origin time		M_L	Lat.	Long.	Zone	ϕ	δ	ϕ	δ	ϕ	δ	L	ϕ	δ	L
61	11/83	1983	11240014	4.7	37.05	36.11	DST	21	184	6	91	70	316	−10	80	50	−160
62*	3/84	1984	03292136	4.9	30.18	32.38	Egp	20	113	7	20	70	245	−10	80	338	−159
63	8/84	1984	08240602	5.3	32.66	35.18	DST	6	61	44	158	65	28	38	55	280	150
64	11/84	1984	11050115	4.0	32.13	35.35	DST	41	116	10	216	70	250	−40	52	356	−154
65	12/84	1984	12181359	4.7	35.29	35.32	CA	1	337	51	69	58	305	42	55	190	140
66	1/85	1985	01250608	4.7	31.91	35.54	DST	45	114	45	294	90	115	90	0	340	135
67	2/85	1985	02281655	4.6	27.72	33.71	SR	7	244	20	151	70	20	10	80	286	159
68*	12/85	1985	12311942	5.3	28.95	35.05	Elt	41	29	2	297	64	261	−146	60	155	−30
69*	7/86	1986	07071417	4.6	34.8	33.67	CA	6	303	53	204	60	331	132	50	90	40
70	11/86	1986	11262308	4.3	35.93	30.77	CA	15	283	48	31	70	255	50	43	142	150
71	1/87	1987	01151119	5.1	34.63	33.86	CA	15	8	62	245	35	160	50	63	25	114
72	2/87	1987	02180534	4.7	34.9	32.26	CA	2	42	58	309	55	70	130	51	194	47
73	4/87	1987	04272041	4.2	31.27	35.47	DST	0	325	14	55	80	190	170	80	281	10
74	6/87	1987	06160617	4.7	35.55	35.25	CA	55	53	30	266	77	253	−105	20	125	−40
75*	9/87	1987	09031239	5.0	35.91	30.61	CA	14	140	27	43	60	275	10	81	179	149
76	10/87	1987	10231632	4.1	31.19	35.34	DST	63	286	24	82	70	90	−80	22	242	−115
77*	11/87	1987	11090750	4.4	34.72	32.88	CA	36	347	46	129	85	330	70	20	226	165
78	1/88	1988	01300300	4.1	32.2	35.5	DST	17	308	3	39	75	175	−170	80	82	−15
79	3/89	1989	03310044	5.4	31.88	37.46	Srn	5	322	81	192	40	135	80	50	327	98
80	9/89	1989	09090516	4.1	28.57	34.82	Elt	74	320	3	219	50	205	−110	43	54	−67
81	10/92	1992	10121309	5.9	29.9	31	Egp	52	142	11	37	65	10	−130	46	253	−35

Abbreviations: Each event is noted by its symbol on the seismotectonic maps; origin time of year, month, day, hour and minute; local magnitude; and epicentral coordinates. Zones are: CA, Cypriot Arc; DST, Dead Sea Transform; Egp, Egypt; Elt, Gulf of Elat (Aqaba); Med, Mediterranean Sea; NMTJ, Northeast Mediterranean Triple Junction; Plm, Palmyride fold belt; Sin, Sinai; Srn, Wadi Sirhan; SR, Suez Rift. Mechanisms are given by the Plunge (ϕ) and the Trend (δ) of the Pressure (P) and Tension (T) axes; and Plunge (ϕ), Trend (δ) and Rake (L) of the two nodal planes. '*' denotes poor quality solutions that are presented here because they agree with the local tectonics (see text for explanation).

360 $M_L \geq 4$ earthquakes that occurred during the years 1900–1992 were found to have at least 10 polarity readings.

While evaluating the data and the solutions, and because we mostly dealt with solutions based on little data, we realized the importance of additional quality factors beside the statistics given by the FPFIT program (Reasenberg & Oppenheimer 1985). Table 3 lists the definition of all the quality factors and Table 4 summarizes the reliability of each focal solution. The factors that we used are as follows.

(1) Statistics calculated by the FPFIT program (Reasenberg & Oppenheimer 1985).

(a) QF, quality code summarizeing the degree to which the solution fits the data (0 = complete misfit, 1 = excellent fit).
(b) STDR, estimator sensitive to the distribution of the data on the focal sphere, relative to the radiation pattern. The closer the data are to the nodal planes, the less robust the solution is, involving values of STDR < 0.5.
(c) QP, quality code that summarizes the range of uncertainties of the strike, dip and rake in a solution.

(2) Additional quality estimators defined in this study.

(a) AD, azimuthal distribution of the stations on the focal sphere. The more widely the data are spread, the better the focal sphere is represented.
(b) RPS, reversed polarity stations. As the number of stations with reversed polarity recordings increases, the reliability of the solution decreases. Previous researchers (e.g. Hodgeson & Adams 1958; Oppenheimer *et al.* 1988) recognized that a certain percentage of the first-motion readings of *P*-wave arrivals did not fit the solution. This is also clearly seen in nuclear explosion records, where some stations show dilatation instead of compression (Table 5). Here we selected several events to examine the presence of possible reversed-polarity stations. We checked *P*-wave arrival records of the relevant stations in nuclear explosion events, as documented in the ISS and ISC Bulletins. A station becomes questionable if it constantly shows dilatation readings in nuclear explosions occurring before and after a given earthquake.
(c) CS, critical stations. We found that in certain configurations the solution is critically dependent on the polarity of one or a few stations. Reversing the polarity or removing that particular station will dramatically change the solution, while with any other station the mechanism remains stable. Since a certain percentage of reversed polarity stations does exist, the stability of the solution degrades as the number of critical stations increases.
(d) CNP, constraints on nodal planes. The closer the stations that fit a solution are to the nodal planes, the better they constrain the planes. While the STDR factor, as described above, weighs the overall pattern of the data distributed on the focal sphere in relation to the best-fitted double couple, this estimator searches for certain readings that constrain the position of the nodal planes. In a sense CNP reflects the advantage of having stations close to the nodal planes.

To each of these estimators we assigned the values (points): 1, good, 2, fair and 3, poor (Table 3). The sum of these points then defined the reliability of a solution ('Total' column in Table 4). In the case of multiple solutions to an event, the best one (fewer 'bad' points), according to our procedure, was chosen.

Overall, an accepted solution was required to have:

(1) at least ten polarity readings;

Table 2. Parameters of CMT solutions done by Harvard (#.C) and waveform inversions by Hofstetter (#.H). Symbol, origin time, location and zones, are as in Table 1. Magnitude is m_b according to NEIS, or M_W (*) if taken from Hofstetter *et al.* (2003). Mechanisms are given by Harvard conventions: strike, dip and slip of the two planes. Scalar moment (Sm) is given by abscissa and exponent.

Event							Best double couple						
No	Symbol	Origin time	m_b	Long.	Lat.	Zone	Str1	Dip1	Slip1	Str2	Dip2	Slip2	Sm
82.C	6/77	1977 06011254	5.6	31.3	36.16	CA	132	64	155	234	67	29	3.40 e24
83.C	5/79	1979 05280927	5.8	31.72	36.45	CA	48	27	−133	274	71	−71	9.48 e24
84.C	12/79a	1979 12280309	5.1	35.85	37.52	NMTJ	141	90	180	231	90	0	1.47 e24
85.C	12/79b	1979 12310621	5.3	31.49	36.22	CA	67	23	−149	308	79	−70	4.18 e24
86.C	5/80	1980 05020530	5.2	29.8	35.68	CA	104	8	−72	266	82	−93	7.42 e24
87.C	4/81	1981 04261413	5.3	30.65	36.53	CA	178	30	4	84	88	120	3.51 e24
88.C	7/85	1985 07222132	5.3	28.27	34.37	Med	67	48	−34	181	65	−133	7.33 e23
89.C	10/86	1986 10021012	5.4	28.31	34.82	CA	99	37	−53	236	61	−114	8.95 e23
90.C	6/89	1989 06240309	4.9	35.93	36.72	NMTJ	203	28	−93	27	62	−88	5.04 e23
91.C	4/91	1991 04100108	5.2	36.14	37.31	NMTJ	160	27	−136	29	72	−70	12.91e23
92.C	10/91	1991 10181404	5.2	28.46	35.76	CA	341	73	177	72	87	17	4.49 e23
93.C	12/91	1991 12052021	5.0	31.79	36.13	CA	66	20	−89	245	70	−90	7.05 e23
94.C	3/93	1992 03221103	5.3	34.38	34.7	CA	343	27	133	117	71	71	1.43 e24
95.H	8/93a	1993 08031243	5.8	34.57	28.78	DST	165	35	−96	8	55	−86	9.30 e24
96.H	8/93b	1993 08031633	5.4	34.59	28.79	DST	115	37	−160	9	78	−55	1.80 e24
97.C	2/95	1995 02232110	5.7	32.23	35.02	CA	239	21	140	6	77	73	8.06 e24
98.C	5/95	1995 05290458	5.2	32.19	34.99	CA	224	20	132	0	76	76	11.11 e23
99.H	11/95a	1995 11220415	6.2	34.8	28.81	DST	202	77	−15	295	75	−167	7.70 e26
100.H	11/95b	1995 11221247	*5.1	34.75	28.45	Elt	20	89	−12	110	78	−179	5.00 e23
101.H	11/95c	1995 11222216	*5.2	34.72	28.55	Elt	288	88	168	18	78	2	6.98 e23
102.H	11/95d	1995 11231807	*5.6	34.75	29.33	Elt	15	86	7	284	83	176	2.66 e24
103.H	12/95	1995 12110132	*5.2	34.86	29.20	Elt	339	79	164	72	74	12	6.79 e23
104.H	2/96	1996 02210459	*5.2	34.71	28.86	Elt	328	48	−97	159	42	−82	6.25 e23
105.C	10/96a	1996 10091310	6.3	32.1	34.53	CA	48	77	170	140	80	13	1.85 e26
106.C	10/96b	1996 10100110	5.4	32.12	34.5	CA	139	53	12	41	80	143	4.66 e24
107.C	10/96c	1996 10100454	5.0	32.16	34.67	CA	147	62	4	55	87	152	7.09 e23
108.C	11/96	1996 11270044	5.0	32.04	34.48	CA	62	48	−168	323	81	−43	12.78 e23
109.H	12/96a	1996 12200721	4.1	33.15	27.63	SR	128	56	−73	280	38	−113	4.24 e22
110.C	12/96b	1996 12242216	4.9	38.58	34.29	Plm	240	75	9	147	81	165	2.03 e24
111.C	1/97a	1997 01131019	5.2	32.31	34.29	CA	97	76	−11	190	79	−166	3.98 e24
112.C	1/97b	1997 01221757	5.3	35.94	36.18	NMTJ	243	39	−15	345	81	−128	4.32 e24
113.H	5/98	1998 05281833	5.3	28.06	31.47	Med	175	47	112	325	47	69	1.98 e24
114.C	6/98	1998 06271355	6.6	35.31	36.88	NMTJ	321	75	171	53	81	15	2.96 e25
115.C	7/98	1998 07040215	5.4	35.32	36.87	NMTJ	72	55	8	338	84	145	15.87 e23
116.C	5/99	1999 05251715	5.6	32.13	34.48	CA	14	53	165	113	78	38	2.60 e24
117.C	8/99	1999 08110428	5.6	32.94	34.79	CA	303	42	124	80	56	63	2.93 e24
118.C	6/01	2001 06251328	5.6	35.82	36.91	NMTJ	184	15	−88	2	75	−90	1.5 e24

Table 3. List of criteria used to define the weight of the quality parameters that determine the reliability of the fault plane solutions. See the text for explanations.

Quality parameter		Weight		
		1, good	2, fair	3, poor
QF	Degree of misfit	0.025 >	0.025 ≤ QF ≤ 0.1	0.1 <
STDR	Station distribution	0.55 <	0.55 ≥ STDR ≥ 0.45	0.45 >
QP	Range of the solution	20° >	20° ≤ QP ≤ 40°	40° <
AD	Azimuthal distribution	180° <	180° > AD > 90°	90° >
RPS	Reversed polarity stations	10 per cent >	10 per cent ≤ RPS ≤ 30 per cent	30 per cent <
CS	Critical stations	0	1 ≤ CS ≤ 4	4 <
CNP	Constraint on nodal planes	CNP = 2	CNP = 1	CNP = 0

(2) azimuthal coverage of station readings on the focal sphere greater than 90°;

(3) less than 20 per cent of phase readings that do not fit the solution;

(4) a total sum of the values (points) of the reliability estimators of at least fair (12–16 points), where good solutions (7–11 points) were given less weight and poor solutions (17–21 points) were rejected.

On the whole, we calculated 81 solutions (Table 1 and Appendix A), of which 48 are presented here for the first time. References to the other previously published solutions are cited in Appendix

Table 4. Reliability of the fault plane solutions that were based on first *P*-wave arrivals. Event parameters are as in Table 1. The quality parameters QF, STDR, QP, CS, RPS, AD and CNP are as explained in the text and Table 2. 'No of obs' is the number of first-motion observations and 'Total' is the sum of all quality parameters. The lower the sum the better the solution is. '*' denotes poor-quality solutions (see the text and Appendix B for explanations).

Event						Quality parameters (1 = good, 2 = fair, 3 = poor)								
No	Symbol	Origin time		M_L	Zone	No of obs.	QF	STDR	QP	CS	RPS	AD	CNP	Total
1	8/40a	1940	08161602	5.1	CA	8	1	2	1	3	–	3	3	13
2	8/40b	1940	08161823	5.0	CA	10	1	1	2	3	–	3	3	13
3	1/41	1941	01200337	6.0	CA	10	1	2	2	3	–	2	2	12
4*	9/45	1945	09021154	6.4	Med	8	1	2	2	3	–	3	2	13
5	4/51	1951	04082138	5.7	CA	19	3	2	1	2	–	1	2	11
6	9/53	1953	09100406	6.2	CA	34	1	2	1	2	–	2	2	10
7	9/55	1955	09120609	6.1	Med	49	3	1	2	1	–	1	2	10
8	3/56a	1956	03161932	5.2	DST	12	1	3	1	3	1	2	1	12
9	3/56b	1956	03161943	5.5	DST	11	3	3	2	3	1	2	2	16
10	12/56	1956	12181753	5.2	DST	16	3	2	1	3	1	2	2	14
11*	6/59	1959	06131201	5.5	CA	8	3	1	1	3	–	3	2	13
12	9/61	1961	09150146	6.0	CA	63	3	1	1	1	2	1	1	10
13	9/63	1963	09120818	5.0	CA	36	3	1	1	1	2	1	1	10
14*	1/65	1965	01251218	4.7	CA	6	3	2	2	3	3	3	2	18
15	4/66	1966	04081346	4.8	CA	8	3	3	1	3	–	1	2	13
16*	4/67a	1967	04071707	4.8	NMTJ	24	3	3	1	2	3	2	2	16
17*	4/67b	1967	04071833	4.9	NMTJ	39	3	3	1	2	2	1	2	14
18	6/67	1967	06151456	4.6	CA	14	3	3	1	3	3	1	1	15
19	3/68	1968	03261937	4.8	DST	10	1	3	1	3	3	2	1	14
20	11/68	1968	11061341	4.8	CA	39	3	1	1	1	–	1	1	8
21*	3/69a	1969	03241154	5.0	SR	29	3	1	1	2	3	1	2	13
22*	3/69b	1969	03241250	4.8	SR	22	3	3	1	3	–	3	2	15
23*	3/69c	1969	03270615	4.7	SR	9	3	1	2	3	3	2	2	16
24	3/69d	1969	03310716	6.6	SR	117	3	1	2	1	–	1	2	10
25	3/69e	1969	03312144	4.9	SR	19	3	1	2	2	3	2	2	15
26	4/69a	1969	04041218	4.7	SR	11	3	1	1	3	1	2	2	13
27	4/69b	1969	04081031	5.0	SR	24	3	1	2	1	3	2	2	14
28	4/69c	1969	04231337	4.9	SR	26	3	3	1	3	2	2	1	15
29	5/69	1969	05100927	4.8	SR	12	1	1	2	1	–	1	2	8
30*	12/69	1969	12300510	4.8	SR	11	3	1	2	2	1	3	2	15
31	4/70	1970	04280320	4.8	SR	23	3	3	1	2	2	1	1	13
32*	7/70	1970	07011550	4.8	CA	8	3	1	1	3	–	2	2	12
33	10/70	1970	10051453	4.8	Plm	14	3	1	1	2	–	1	2	10
34	12/70	1970	12192244	4.6	SR	11	3	1	1	3	–	2	2	12
35	4/71	1971	04162127	4.6	DST	15	3	3	1	2	–	2	2	13
36	6/71	1971	06290908	5.0	NMTJ	24	3	1	1	1	–	1	2	9
37	7/71a	1971	07082340	5.1	SR	12	3	1	1	3	3	2	2	15
38	7/71b	1971	07112012	5.1	NMTJ	29	3	1	2	2	2	1	2	13
39	8/71	1971	08170429	4.9	NMTJ	26	3	1	1	2	–	1	2	12
40	1/72	1972	01120815	5.0	SR	19	3	1	1	2	1	2	2	12
41	6/72	1972	06280949	5.5	SR	82	3	1	1	1	–	1	2	9
42*	4/74	1974	04292005	5.2	Egp	29	3	3	1	2	2	1	1	13
43*	1/75a	1975	01010030	5.2	NMTJ	27	3	1	1	2	–	1	2	10
44	1/75b	1975	01282112	4.6	CA	16	1	2	1	1	–	1	2	8
45	1/76a	1976	01121750	5.0	CA	42	3	3	1	2	–	1	1	11
46	1/76b	1976	01122019	4.9	CA	11	2	3	1	3	–	2	2	13
47	1/76c	1976	01262244	4.6	CA	21	3	3	1	1	–	2	2	12
48	2/78	1978	02092110	4.5	NMTJ	15	2	3	1	2	–	1	2	11
49	4/79a	1979	04042117	4.4	CA	15	3	1	1	2	–	1	2	10
50	4/79b	1979	04231301	5.0	DST	55	3	2	2	2	–	1	1	11
51*	9/79	1979	09201037	4.0	CA	8	1	3	1	3	–	3	2	13
52	1/80	1980	01021252	4.7	EAF	12	2	2	1	2	–	1	2	10
53	2/81	1981	02190241	4.7	DST	17	3	3	1	3	–	2	2	14
54	6/81	1981	06300759	4.7	DST	10	3	1	1	2	–	1	2	10
55	8/81	1981	08100521	4.6	CA	21	3	1	1	2	–	1	2	10
56*	3/82	1982	03231048	4.7	Elt	18	3	2	2	2	–	3	2	14
57	5/82	1982	05200328	4.6	CA	33	3	3	2	2	–	1	1	12
58	6/83a	1983	06030204	4.9	DST	19	1	1	2	1	–	2	2	9

Table 4. (*Continued.*)

Event						Quality parameters (1 = good, 2 = fair, 3 = poor)								
No	Symbol	Origin time		M_L	Zone	No of obs.	QF	STDR	QP	CS	RPS	AD	CNP	Total
59	6/83b	1983	06121200	5.4	SR	64	3	1	2	2	–	1	2	11
60	9/83	1983	09241640	4.6	CA	13	2	3	1	2	–	2	1	11
61	11/83	1983	11240014	4.7	DST	30	3	2	1	2	–	1	1	10
62*	3/84	1984	03292136	4.9	Egp	33	3	3	2	2	–	1	2	13
63	8/84	1984	08240602	5.3	DST	73	3	3	1	1	–	1	1	10
64	11/84	1984	11050115	4.0	DST	13	2	1	1	2	–	2	2	10
65	12/84	1984	12181359	4.7	CA	25	3	3	1	2	–	2	2	13
66	1/85	1985	01250608	4.7	DST	32	2	1	1	2	–	1	2	9
67	2/85	1985	02281655	4.6	SR	15	3	3	1	3	–	1	2	13
68*	12/85	1985	12311942	5.3	Elt	33	3	1	1	2	–	3	2	12
69*	7/86	1986	07071417	4.6	CA	33	3	3	1	1	–	1	1	10
70	11/86	1986	11262308	4.3	CA	21	3	3	1	2	–	2	2	13
71	1/87	1987	01151119	5.1	CA	71	3	1	1	2	–	1	2	10
72	2/87	1987	02180534	4.7	CA	44	3	1	1	2	–	2	2	11
73	4/87	1987	04272041	4.2	DST	27	3	1	1	1	–	1	1	8
74	6/87	1987	06160617	4.7	CA	10	2	3	1	1	–	2	2	11
75*	9/87	1987	09031239	5.0	CA	96	3	2	1	1	–	1	1	9
76	10/87	1987	10231632	4.1	DST	28	3	2	1	2	–	1	1	10
77*	11/87	1987	11090750	4.4	CA	23	3	1	2	2	–	1	3	12
78	1/88	1988	01300300	4.1	DST	23	2	1	1	1	–	1	1	7
79	3/89	1989	03310044	5.4	Srn	60	2	1	1	1	–	1	2	8
80	9/89	1989	09090516	4.1	Elt	13	3	2	1	2	–	2	2	12
81*	10/92	1992	10121309	5.9	Egp	180	3	3	1	1	–	1	3	12

Table 5. Examples of dilatational *P*-wave onsets in nuclear explosions. We counted the number of compressional and dilatational records of each event as appears in the ISS and ISC Bulletins, and calculated the percentage of dilatational readings. 'Origin time' as in Table 1.

Origin time	m_b	Test area	Compression records	Dilatation records	Percentage of dilatation records
196310201259	?	Sahara	18	12	40
196404242010	?	Nevada	10	3	23
196405160600	5.6	Semi-palatinsk	26	9	25
197012230700	6	Caspian Sea	110	15	12
197405310327	5.9	Semi-palatinsk	93	9	9
198009140243	6.2	Semi-palatinsk	189	13	6
198208051400	5.7	Nevada	151	12	7
198706050500	6.8	Lop-Nor, China	259	32	11
198810121400	6.1	Nevada	160	20	11

B. Among the solutions that did not meet the above-mentioned requirements, there are 19 mechanisms that seemed to agree with the local tectonics or were similar to other nearby accepted solutions (Appendix B). Since the number of potential solutions over the area studied is limited, we still discuss these 'doubtful' mechanisms, though they were excluded from statistical characterization and limited to tectonic interpretations (they appear grey on the seismotectonic maps).

2.2 Focal solutions based on waveform inversion

With the increasing number of teleseismic and regional broad-band stations in recent years, the availability of waveform inversion solutions and their higher reliability than the first-motion solutions led us to add the relevant solutions to our list. We compared our first-motion solutions (Table 1) of relatively moderate to strong events 4/79b (#50), 8/84 (#63) and 10/92 (#81) with the relevant Harvard Centroid Moment Tensor (CMT) solutions (Larson 1999), and found that they show the same sense of motion with quite similar orientations of the fault planes. We also found a good agreement among nearby CMT solutions and in most cases the solutions agree with the local tectonic setting. However, where available, we used Hofstetter *et al.* (2003) solutions since their waveform inversion is more refined. It includes a two-step procedure: the first step served as a rough estimate of the mechanism while the second step, by using a grid estimate over a wide range of values, was a refinement of the first estimate.

Altogether we added to our list 37 solutions of events that occurred in the study area during 1977–2001 (Table 2), as found in the 'Harvard Seismology CMT Catalogue Search' (Larson 1999) and appear in Hofstetter *et al.* (2003) for the $M_W \geq 5.0$ aftershocks of the 1995 November 22 Gulf of Aqaba earthquake.

3 DISCUSSION

The pattern of seismicity during the previous century is presented in Fig. 1. It is based on Salamon *et al.* (1996), and updated with additional $M_L \geq 4$ recorded events that occurred in the study area during the last decade, as catalogued in the on-line database of the ISC (1964–1993, 1991, 2000), NEIC and PDE bulletins. Although the seismicity in the last decade was the most active of the last century, it still agrees with the configuration of the seismogenic belt of the Sinai subplate, which was based on the seismicity of the first 90 yr.

In the following sections we describe in detail the mechanisms along the subplate margins and the way they express the deformation associated with the Sinai subplate borders.

3.1 The Dead Sea Transform

The Dead Sea Transform, which forms the Arabian–Sinai plate boundary, extends from the Sinai Triple Junction to the NMTJ (Fig. 1). The overall morphology and development of typical secondary structures along the transform attest to its recent activity. Its principal left-lateral sense of motion is recognized by minor pull-aparts in young sediments (Garfunkel *et al.* 1981), cut and offset of drainage lines and man-made structures (e.g. Reches & Hoexter 1981; Marco *et al.* 1997, 2000; Niemi 1997; Zilberman *et al.* 2000; Amit *et al.* 1999; Zhang & Niemi 1999; Klinger *et al.* 2000a,b; Gomez *et al.* 2001).

The current seismicity associated with the transform supports these findings. It is concentrated along the southern leaky part of the DST, especially in the deep depressions of the Gulf of Aqaba and the Dead Sea, but there has been little activity along the Arava Valley. North of the Carmel-Fari'a branching fault system, the seismic activity is scattered on the western side of the transform ((Fig. 2 Salamon *et al.* 1996). In this area young lateral motion along the main transform fault is demonstrated by the offset of buried drainage lines (Marco *et al.* 2000) and the offset of the walls of a crusader fortress built right on the active fault line (Marco *et al.* 1997; Ellenblum *et al.* 1998). More to the north, there was very little seismic activity over the past century along the Yammouneh restraining bend and its northward continuation.

Over the last century most of the seismic moment was released by a few large events, and these in fact record the main motion along the transform (Fig. 1): (a) an event in 1918 September, $M_L = 6.2$, near the Syrian segments, about which little is known; (b) the destructive shock in 1927 July, $M_L = 6.2$, in the northern Dead Sea basin; and (c) the Gulf of Aqaba (Nuweiba) event, 1995 November, $M_W = 7.2$.

There are no available first-motion data of the 1918 September and 1927 July events. However, based on surface wave data, Ben-Menahem *et al.* (1976) obtained a focal mechanism on showing left-lateral motion on a subvertical fault striking 010°, i.e. parallel to the transform in that area. The good data concerning the 1995 November event yielded mechanism of a left-lateral motion on a steep fault striking 202°. Thus, the major shocks in the last century record the predominant left-lateral transform motion.

Most of the mechanisms we were able to compute are of smaller events, however, and they are concentrated especially along the southern part of the transform. The most striking result here is the variety of focal mechanisms of these events, reflecting a much more complicated picture. As these are relatively weak events, they record second-order motions along the transform, but their varied mechanisms provide valuable insights into the complexity of the transform and the secondary structures along it.

As noted, the DST is not simply a straight line of pure strike-slip motion, but much of its southern half is leaky, i.e. arcuate transtensional fracture, with minor irregularities, which produce local transpression (Garfunkel 1981). Thus, oblique slip took place on some major faults, while normal-slip faults developed along others—both longitudinal and transverse (Garfunkel & Ben-Avraham 2001). It is these complexities that seem to be recorded by the focal mechanisms of the weaker events. We shall discuss first the occurrence of the mechanisms on the plate border and then their occurrence along the plate margins.

3.1.1 Focal mechanisms along the Dead Sea Transform

In principle, a mechanism that reflects plate motion should depend on the angle between the local strike of the plate border and the direction of the relative motion between the adjacent plates. When these two directions coincide, in the case of a transform a pure strike-slip is expected, as we observe in events 4/79b, 4/87 and 1/88. When the two strikes differ, transtension or transpression should occur. This seems to be the cause of the 1/85 transpressional mechanism near Jericho, which is a compressional region (Garfunkel 1981; Gardosh *et al.* 1990; Rotstein *et al.* 1991). Thus local variations in the geometry along the transform determine the type of the earthquake mechanism there.

Most of the mechanisms in the Gulf of Aqaba are of aftershocks of the 11/95a event. Until then, the reliable solutions were only of the 9/89 and the 8/93a $M_b = 5.8$ extensional events (Fig. 2). The other 3/82 and 12/85 solutions also record normal faulting, but are presented here despite their high errors because they agree with the local tectonics. These events lack the expected principal shear component and we relate this to the faults that form the boundaries of the major basins in the gulf (Ben-Avraham *et al.* 1979; Garfunkel & Ben-Avraham 2001). They reflect the component of extension normal to the transform, an idea originated with Quennell (1959), and then elaborated by Freund *et al.* (1970), Garfunkel (1981), Lyberis (1988) and Ben-Avraham & Zoback (1992) and others. It is interesting to note Bosworth & Strecker's (1997) observations of normal faulting in the alluvial fan near Nuweiba. Their field evidence seems to support the idea of extension normal to the transform as well. Alamari *et al.* (1991) presented evidence for normal and shear mechanisms of microseismic events, yet these alone do not show predominance of lateral faulting, as is demonstrated by the large events.

Nevertheless, the occurrence of the strongest recorded earthquake in the Gulf on 1995 November 22, $M_W = 7.2$ (11/95a), clarified the seismotectonic picture: most of the seismic moment along this segment of the transform was released by left-lateral motion. It was followed by an intense swarm of aftershocks that lasted over a year, with a peak magnitude of $M_W = 5.6$ (11/95d). Some aftershocks (e.g. 11/95b, 11/95c, 11/95d, Fig. 2) show predominantly left-lateral motion on steep faults, striking more or less along the course of the transform segment, while the 2/96 aftershock records a normal motion. It is interesting to note the association of extensional activity (events 12/85, 8/93a, and 8/93b) prior to the release of a strong shear event (11/95a) within a large rhomb-shaped basin. It may typify the pattern of stress release in the Gulf of Aqaba region.

The normal mechanisms of 12/56 and 10/87 near the Dead Sea cannot be related to the lateral motion along the transform. They seem to record the activity of the longitudinal N–S-striking normal

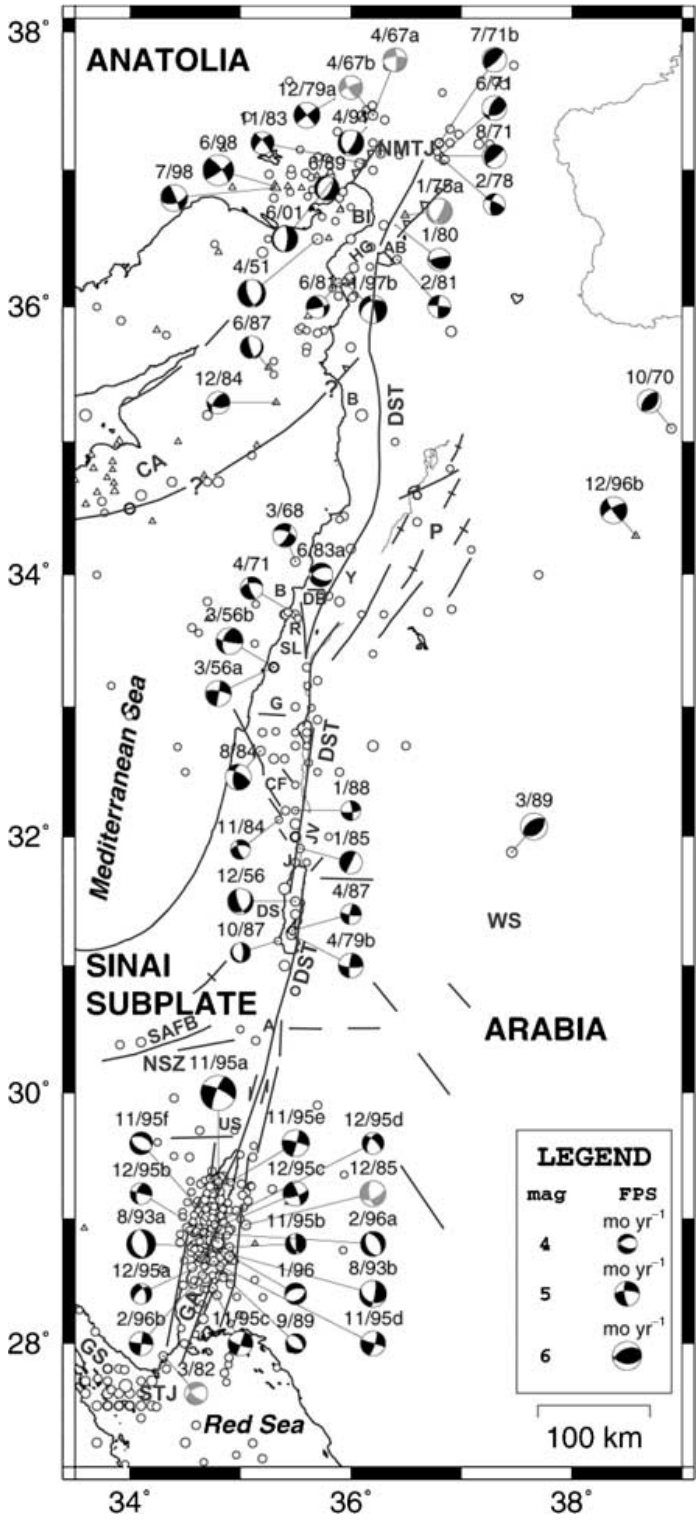

Figure 2. Seismotectonic map of the Dead Sea Transform. Fault plane and waveform inversion solutions are presented with lower-hemisphere equal-area projection: white quadrants for compression and black for dilatation. Mechanisms are symbolized by the month and year of the origin time (e.g. '4/79' means 1979 April or 197904. . .). The size of the 'beach ball' is relative to the magnitude. Grey spheres indicate doubtful solutions. Mechanism parameters, reliability and notes are as in Tables 1 , 2, 4 and Appendices A and B. Plate borders are the Dead Sea Transform (DST) and the Cypriot Arc (CA). Geological elements and localities: A, Arava Valley; AB, Amik Basin; Ba, Baniyas; Be, Beirut; BI, Bay of Iskenderun; CF, Carmel–Faria fault system; DB, Dahr el Beider; DS, Dead Sea; G, Galilee; GA, Gulf of Aqaba; GS, Gulf of Suez; J, Jericho; JV, Jordan Valley; NMTJ, Northeast Mediterranean Triple Junction; NSZ, Negev Shear Zone; R, Roum fault; SAFB, Syrian Arc Fold Belt (including P, Palmyrides); SL, South Lebanon; STJ, Sinai Triple Junction; US, Uvda & Sayarim grabens; WS, Wadi Sirhan; Y, Yammouneh bend.

faults that extend along the margins of the Dead Sea depression and other parts of the transform. Field evidence shows that these are active faults (Agnon 1981; Garfunkel *et al.* 1981; Raz 1983; Gardosh *et al.* 1990) and some even have a minor dextral component (Mor 1987), which is also found in our mechanisms.

The event of 2/81, south of the NMTJ (Fig. 2), shows dextral motion on the N–S-striking nodal plane and therefore could not be explained in this manner. It might, however, reflect distributed complex deformation near the transform, such as the Miocene deformation in the Galilee and southern Lebanon (Ron & Eyal 1985). Alternatively, if the E–W-striking nodal plane is the fault, this mechanism may be related to the East Anatolian branch of the triple junction, or even to the CA.

3.1.2 Mechanisms west of the transform, along the eastern Sinai subplate margins

Most of the marginal seismicity occurs west of the transform, between the Carmel-Fari'a fault system and Beirut (Fig. 2). Freund *et al.* (1970) and Ron & Eyal (1985) already noticed the association in time and space of the deformation of this region with the transform. They ascribed it to the Yammouneh bend that restrains the relative motion between Arabia and Sinai and produces a complex fault pattern, which as yet, does not enable a simple explanation of the variety of the marginal mechanisms.

A possible source of both 3/56a and 3/56b, the 4/71 and the 1992 September, $M_L = 3.7$ (IPRG Bulletin 1992) events is the Roum fault (Fig. 2) that branches out from the transform at the southern deflection point of the Yammouneh bend. Thus, these events record a left-lateral motion on an N–S-striking fault. However, we cannot exclude the many right-lateral E–W-striking faults in southern Lebanon (Hancock & Atiya 1979) as an alternative potential source of these events. Just to stress the tectonic complexity of the region, considering the probable mislocation at that time, these events could also have originated on the Yammouneh fault itself. Near Beirut, the extensional 6/83a mechanism may record motion of one of the E–W-striking normal faults of Dahr el Baidar (Hancock & Atiya 1979). For the offshore tremor of 3/68, we are unable to determine the preferred fault plane, as the offshore structures are unknown.

The transpressional mechanism of 8/84 is unexpected (Fig. 2), since its vertical component is not in agreement with the current interpretation of the surface geology. The NW-striking northern segment of the Carmel fault (Figs 1 and 2) shows normal faulting with a left-lateral component (Karcz 1959; De-Sitter 1962; Achmon & Ben-Avraham 1997), while its central segment strikes N–S and shows a left-lateral motion only (Achmon & Ben-Avraham 1997). Rotstein *et al.* (1993) and Hofstetter *et al.* (1996) proposed, on the basis of high-resolution seismic imaging and fault plane solutions, that the present motion on the Carmel fault is left-lateral, with its central segment being a restraining bend that causes the uplift of Mt Carmel. Thus, the surprising transpressional 8/84 mechanism suggests re-examination of the structures associated with the Carmel fault as it apparently cannot be associated with this major seismogenic fault. Extension with a sinistral shear component also appears in the Fari'a graben in mechanism 11/84 (Fig. 2) and is in accord with field evidence (Shaliv 1972).

It is noteworthy that many prominent structures near the transform did not display significant seismic activity during the last century, such as the faults east of the Arava valley (Mt Edom) or the Uvda and Sayarim grabens west of it, which exhibit only sparse microseismicity (IPRG Bulletins 1982–1993; GII Bulletin 1996; van Eck & Hofstetter 1990). The fault system west of the southern Arava, that was active in Pliocene–Pleistocene times (Avni *et al.* 2000), also did not generate any notable seismic activity. Whether these structures are aseismic, or the repeat time of their major seismic events is much longer than a century, is yet to be investigated.

3.1.3 Distribution of strike and rake directions

We examined the distributions of the strike (Fig. 3) and rake (Fig. 4) directions of the nodal planes to see yet another aspect of the degree that the fault mechanisms reflect the tectonics of the DST. We considered both the fault and the auxiliary planes of only the accepted solutions (Table 1), so as to rule out any bias of the doubtful solutions or subjective selection of the preferred 'real' fault planes, although the presence of the auxiliary planes increased the background 'noise' level.

Strike directions of the fault plane mechanisms show a dominant NNW mode, in accordance with the strike of the DST. The other modes are smaller and near the general N, S, E, and W directions (Fig. 3a). When we split this population into a group of events in the north (Fig. 3b) and a group in the Gulf of Aqaba (Fig. 3c), the picture is not dramatically changed, thus stressing the similar nature of the two segments as part of the same tectonic regime. The distribution of strikes for the northern events (Fig. 3b) is the same as for the whole DST. This seems to reflect mostly shear planes parallel to the transform and auxiliary planes normal to it. The dominant mode in the Gulf of Aqaba is parallel to the strike of the DST. The other E–W modes are of the auxiliary planes and may also reflect the extension normal to the transform.

Rake directions show that the DST is a transtensional regime, a combination of a major left-lateral mode and secondary normal and right-lateral modes (Fig. 4a). The expected sinistral shear appears all along the transform (Figs 4b and c) as do the normal modes, which reflects the extensional component of the leaky transform (Garfunkel 1981). The right-lateral mode probably represents the auxiliary planes of the shear mechanisms.

3.1.4 Northeast Mediterranean Triple Junction

Various mechanisms appear at the juncture zone of Sinai, Arabia and Anatolia, where the DST, the East Anatolian Fault and the CA meet (Figs 2 and 5). The overall deformation of the Arabian–Anatolian boundary seems to separate into two components: a left-lateral shear which is absorbed on ENE-striking faults (mechanisms 4/67a, 4/67b, 12/79a, 11/83, 6/98, 7/98); and an NW thrusting on either steep- or shallow-dipping planes (events 6/71, 7/71b, 8/71 and 1/80). This process was previously suggested by McKenzie (1976), Rotstein & Kafka (1982), Kempler & Garfunkel (1991), Lyberis *et al.* (1992) and Jackson (1992), and is clearly demonstrated here on the rake distribution diagram (Fig. 4d). Based on the variety of the focal mechanisms of the recent greatest earthquakes along the East Anatolian Fault, including oblique, normal and reverse faultings, Taymaz *et al.* (1991) were able to calculate the overall slip rate across this fault zone. Furthermore, an extensional regime is found amid the shear and the thrust, possibly related to the Iskendrun Bay, such as the 4/51, 6/89 and 4/91 events. Event 1/75a can be related to the marginal faulting of the Amik Basin (Perincek & Cemen 1990; Lyberis *et al.* 1992; Rojay *et al.* 2001) in the southern Karasu (Hatai) Rift, east of the Iskenderun Bay.

Far less active is the DST branch, where the indistinct 2/81 mechanism (discussed in 3.1.1) was the only one we could find

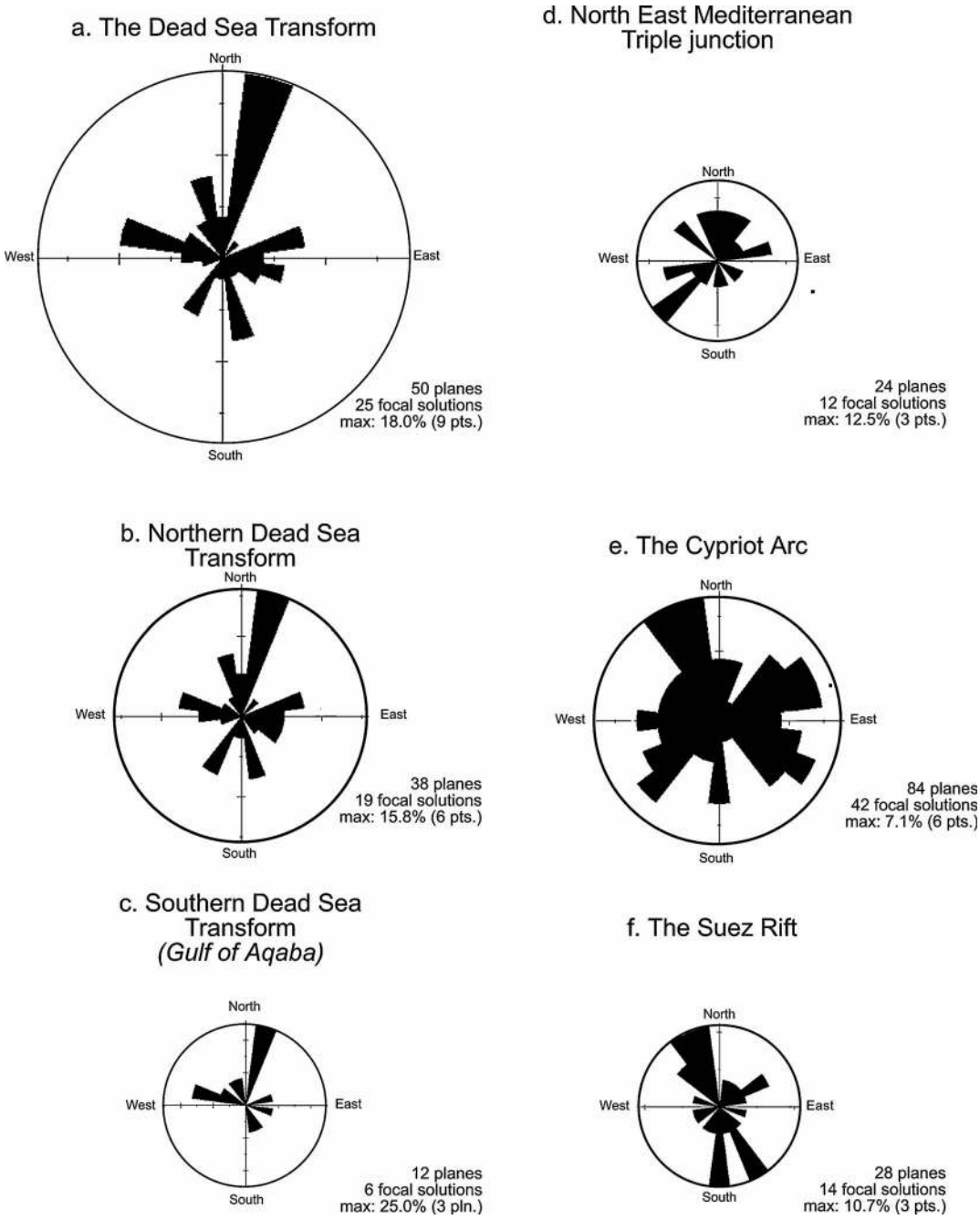

Figure 3. Rose diagram of the strike directions of both the fault and the auxiliary planes. Only the reliable solutions of events that occurred along the Sinai subplate borders are considered. Data are from Table 1.

data for. The intriguing association of extensional mechanisms (4/51 and 6/87) together with left-lateral thrusts (6/81 and 12/84), which seem to be part of the CA, is discussed below (Figs 2 and 5).

The *Strike* direction of mechanisms at the NMTJ are mainly NE and SW, in agreement with the East Anatolian Fault and the CA branches (Fig. 3d). The other directions seem to reflect the auxiliary planes. It is interesting to note though, that the presence of the DST branch is hardly noticeable.

Rake directions interestingly show partitioning of the deformation into a dominant normal faulting and less prominent reverse and shear modes (Fig. 4d). It may echo the complex tectonics near the triple junction. The normal mode reflects the extension in the Gulf of Iskendrun. The other modes seem to express the components of shear along the East Anatolian Fault and compression between Anatolia and Arabia, and thus complement the findings of Taymaz *et al.* (1991) of various mechanisms along the northern part of the Arabia–Anatolia plate boundary.

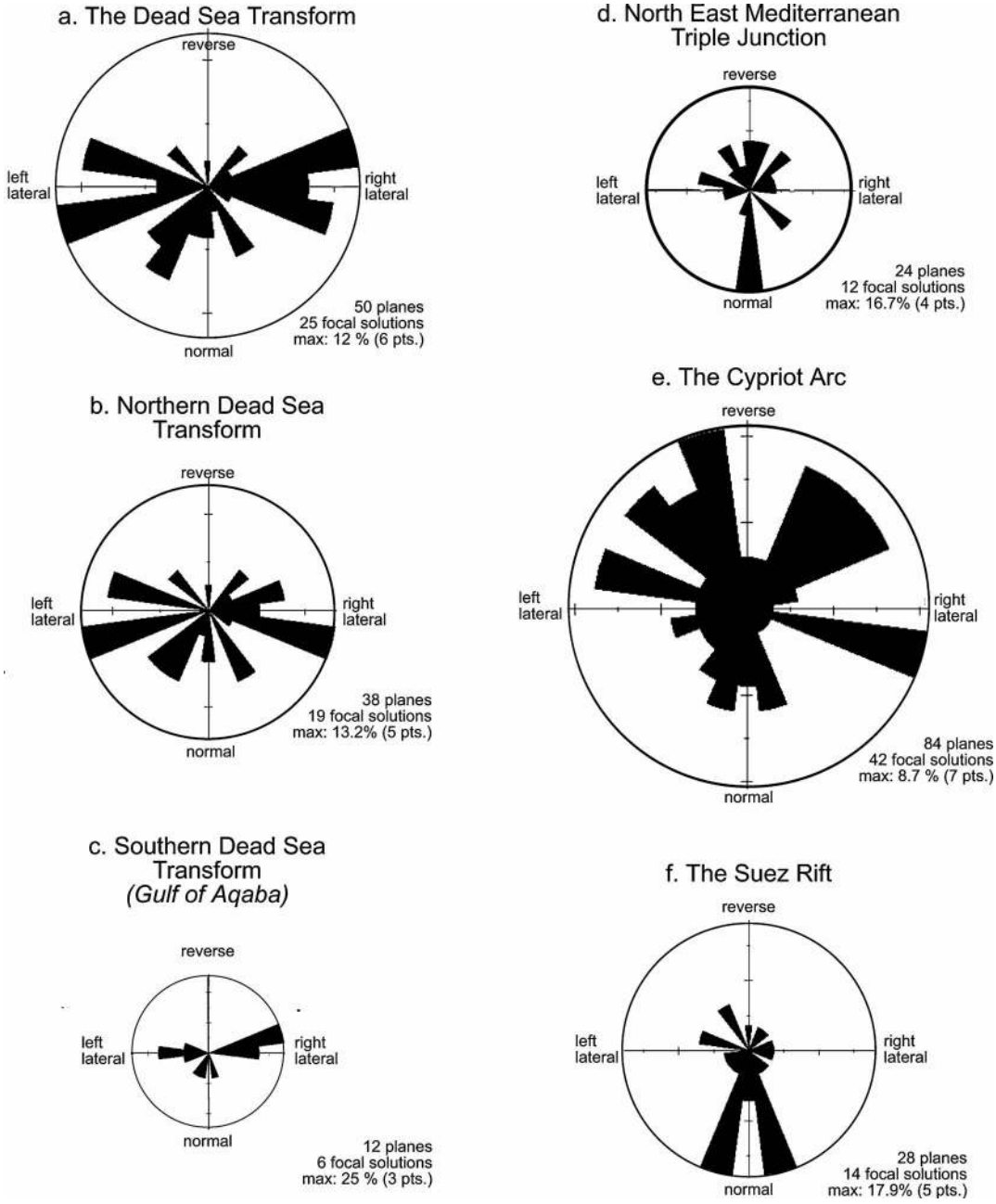

Figure 4. Rose diagram of the rake directions of both the fault and the auxiliary planes. Only the reliable solutions of events that occurred along the Sinai subplate borders are considered. Data are from Table 1. Presentation of rakes on the rose diagram is modified to show: 'up' as reverse faulting, 'down' as normal faulting, 'left' as left-lateral (sinistral) strike-slip faulting and 'right' as right-lateral (dextral) faulting.

3.1.5 Seismic efficiency

In order to estimate the seismic efficiency we consider the following parameters of the DST:

(1) length of 1000 km;
(2) the depth range of the seismogenic zone is 15 km (focal depth of the Gulf of Aqaba event);
(3) the shear modulus is 3×10^{11} dyne cm;
(4) the conservative rate of relative motion is 0.5 cm yr^{-1} (Garfunkel *et al.* 1981).

Then its expected seismic moment release during the previous century should have reached 2.25×10^{27} dyne cm. Applying Shapira's (1988) and Shapira & Hofstetter's (1993) magnitude and moment-magnitude scaling relationships over the seismicity of the past century, we find that the moment actually released did not exceed 40 per cent of the expected sum, confirming previous estimates that revealed a moment deficiency in the last century (Garfunkel *et al.* 1981). Overall, the Gulf of Aqaba event generated 7.7×10^{26} dyne cm (Hofstetter *et al.* 2003), and the remaining events yielded the rest of the moment. The fact that 86 per cent of the total moment actually released during the past century for the entire length of the

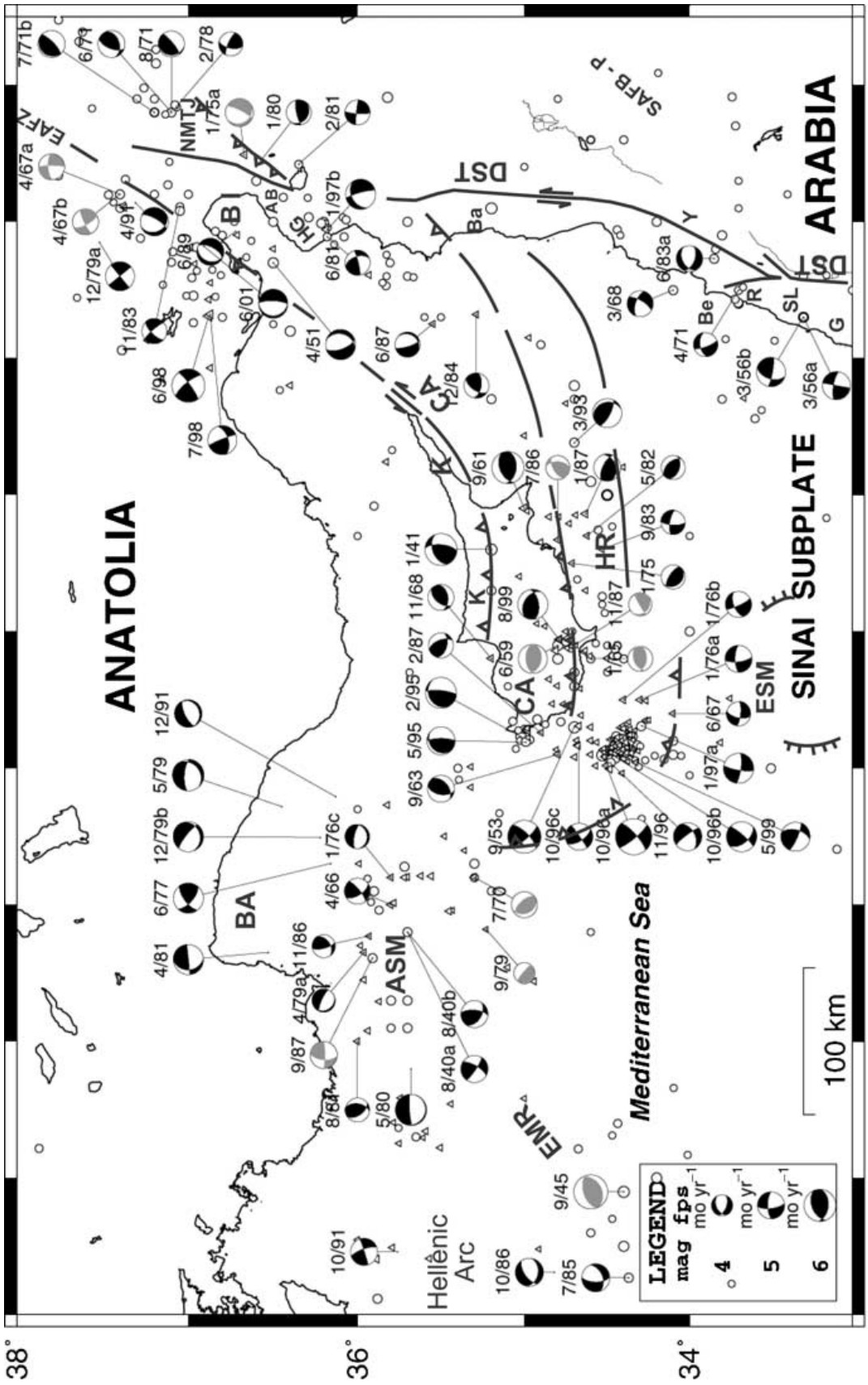

Figure 5. Seismotectonic map of the Cypriot Arc. See Fig. 1 for an explanation of the symbols. Plate borders are the Cypriot Arc (CA) and the Dead Sea Transform (DST). Geological elements and localities: AB, Amik Basin; ASM, Anaximander Seamount; BA, Bay of Antalya; Ba, Baniyas; Be, Beirut; BI, Bay of Iskenderun; EAFZ, East Anatolian Fracture Zone; EMR, East Mediterranean Ridge; ESM, Eratosthenes Seamount; G, Galilee; HR, Hecteaus Rise; K, Kyrenia; NMTJ, Northeast Mediterranean Triple Junction; R, Roum fault; SAFB, Syrian Arc Fold Belt (including P, Palmyrides); SL, South Lebanon; Y, Yammouneh bending.

transform boundary was generated by the shear mechanism of the Gulf of Aqaba event clearly supports the concept of mainly a transformal motion along the Arabian–Sinai plate border and contradicts assumptions of just an extension with a minor shear (Mart 1991; Horowitz 2001).

3.2 The Cypriot Arc

The CA is generally characterized by thrusts and shear mechanisms, with one of their nodal planes being subparallel to the strike of the arc at the epicentre (Fig. 5). The seismicity also follows the arcuate pattern of the arc (Ambraseys & Adams 1993; Papazachos & Papaioannou 1999) and is concentrated in and around southern Cyprus, close to the compressional structures (Robertson *et al.* 1991), and bound in the south by the deformation front of the Hecateaus Rise (Kempler 1994; Vidal *et al.* 2000a). This is clearly borne out by the $M_L \geq 6$ events that generated most of the seismic moment: the thrust events of 1/41 and 9/61, and the transpression events of 9/53 and 10/96a. The seismicity diminishes northward, toward the compressional range of Kyrenia, and ceases just north of Cyprus.

Many of the events with shear mechanisms are located southwest of Cyprus and in the south, where the Eratosthenes Seamount approaches Cyprus (Fig. 5). Yolsal & Taymaz (2002) suggest that the southwestern shear events are related to the dextral Paphos Transform Fault. Most of the solutions in this region (9/53, 10/96abc, 5/99) are associated with a compression component while the 11/96 event which is one of the 10/96 aftershocks, is a transtension event. It is important to note though, that normal faulting is an alternative solution for the 2/95 and 10/96a earthquakes, as calculated by Pinar & Kalafat (1999). Together with the mechanisms calculated by Buyukasikoglu (1980), they concluded that the western vicinity of the Cyprus Island undergoes extensional tectonics. Yolsal & Taymaz (2002) also obtained a normal with a strike-slip mechanism for the 10/96a event, but the other 2/95 and 10/96b were clear thrusts with strike-slip motion.

The other southern events (6/67, 1/76a, 1/76b, 1/97a) probably echo the collision process as the Eratosthenes block is obstructed from being subducted northwards (Rotstein & Kafka 1982; Robertson 1998). Buyukasikoglu (1980) presented normal faulting with a shear component for that region and Kempler & Ben-Avraham (1987) pointed out normal faulting just south of it. All in all, it seems that the convergence process in these regions is dominated by strike-slip mechanisms, yet a detailed mapping is still needed here in order to understand the role of the additional tension or compression components.

East of Cyprus, toward the NMTJ, the seismicity is sparse and the focal mechanisms show both tension and compression with a shear component (Figs 2 and 5). Kempler & Garfunkel (1991) related the simultaneous activation of these transpressional and transtensional systems to the geometry of the plate border, and Vidal *et al.* (2000b,c) showed detailed mapping of these boundary structures. The trend of the eastern CA is in places subparallel to the azimuth of the small circle, which defines the relative motion between Anatolia and Sinai (Africa, in this case). A fault where the strike is slightly deflected from the azimuth of the small circle would receive, in addition to the shear motion, a component of either tension or compression. Our transpressional mechanisms (events 6/81 and 12/84) and the tensional ones (events 4/51 and 6/87) seem to support this explanation.

West of Cyprus, we observe the 7/70 and 9/79 (doubtful) compressional mechanisms, with NW-striking planes, thus possibly indicating the northwestward continuation of the arc. The activity northwest of Cyprus and near the Bay of Antalya is heterogeneous (Fig. 5). We find strike-slip (e.g. 8/40a, 4/66, 6/77), thrust (e.g. 8/40b, 11/86) and normal (e.g. 1/76c, 4/79a, 5/79, 12/91) mechanisms. They may all reflect the complex tectonics of the region, where the CA meets with the Hellenic Arc, near the Bay of Antalya and the Anaximander Seamount. The extension may be related to the formation of the Bay of Antalya (Glover & Robertson 1998) and compression to the subduction near the Bay (Rotstein & Kafka 1982; Buyukasikoglu 1980). The shear may reflect the mechanical difficulty encountered as the Anaximander Seamount approaches Anatolia, much like the Eratosthenes convergence toward Cyprus. Our limited data demonstrate the complexity of the areal tectonic puzzle, yet to be deciphered.

The strong earthquake of 9/45 originated on the Eastern Mediterranean Ridge, already within the Hellenic Arc province, as did also events 7/85, 10/86 and 10/91, which may be associated with the extension processes at the Aegean Sea.

Strike directions of the nodal planes along the arc are not significantly clustered (Fig. 3e). This pattern reflects the geometry of the arc south and southwest of Cyprus. Rake directions, however, seem to be more conclusive: most of the mechanisms are thrusts with a lateral component (Fig. 4e), in accordance with the convergence process along the arc.

3.3 The Suez Rift

The SR which forms the northwestward continuation of the Red Sea across the Sinai Triple Junction, is quite seismogenic (Fig. 1), in agreement with field evidence of recent fault activity (Said 1962; Robson 1971; Garfunkel & Bartov 1977; Jackson *et al.* 1988; Bosworth & Taviani 1996). What seemed to be an aseismic zone at the beginning of the century, released one of the strongest recorded earthquakes around the Sinai subplate (the 3/69d event, $M_L = 6.6$). Most of the solutions presented here are related to its foreshocks and aftershocks (Fig. 6). Our mainshock solution shows an extension normal to the rift axis, in accordance with other previously published solutions (McKenzie *et al.* 1970; Ben-Menahem & Aboodi 1971; Jackson *et al.* 1988). However, Huang & Solomon (1987) found that the mechanisms of the 3/69d and 6/72 events are rotated about 40° anticlockwise relative to the SR axis and concluded that the present extension direction in the SR is NNE–SSW. Bosworth & Taviani (1996) came to a similar conclusion by analysing borehole breakouts and mesoscopic fault arrays. On the other hand, young faults seen in the alluvium near the Gulf usually trend close to the overall elongation of the Gulf, with no data showing an oblique slip component (Garfunkel & Bartov 1977). This implies extension normal to the rift axis. Unfortunately, we are not able to resolve this debate since the dip direction of both the nodal planes in our 3/69d mechanism is not well constrained. Also, the presence of various mechanisms complicates the pattern of the present stress field.

Studies of earthquake clusters show that it is common to find a variety of focal mechanisms associated with strong shears (e.g. Oppenheimer *et al.* 1988) or thrusts (e.g. Hauksson & Jones 1989; Yielding *et al.* 1989). However, the occurrence of thrust solutions together with an extensional mainshock is far less frequent and appears mostly with low-magnitude events (Deschamps & King 1984; Hatzfeld *et al.* 1986/87; Lyon-Caen *et al.* 1988). Some of our newly calculated aftershock mechanisms reveal an additional significant shear (4/69c and 4/70) and even thrust (3/69d and 4/69b) components (Fig. 6). Hurukawa *et al.* (2001) also found great diversity of

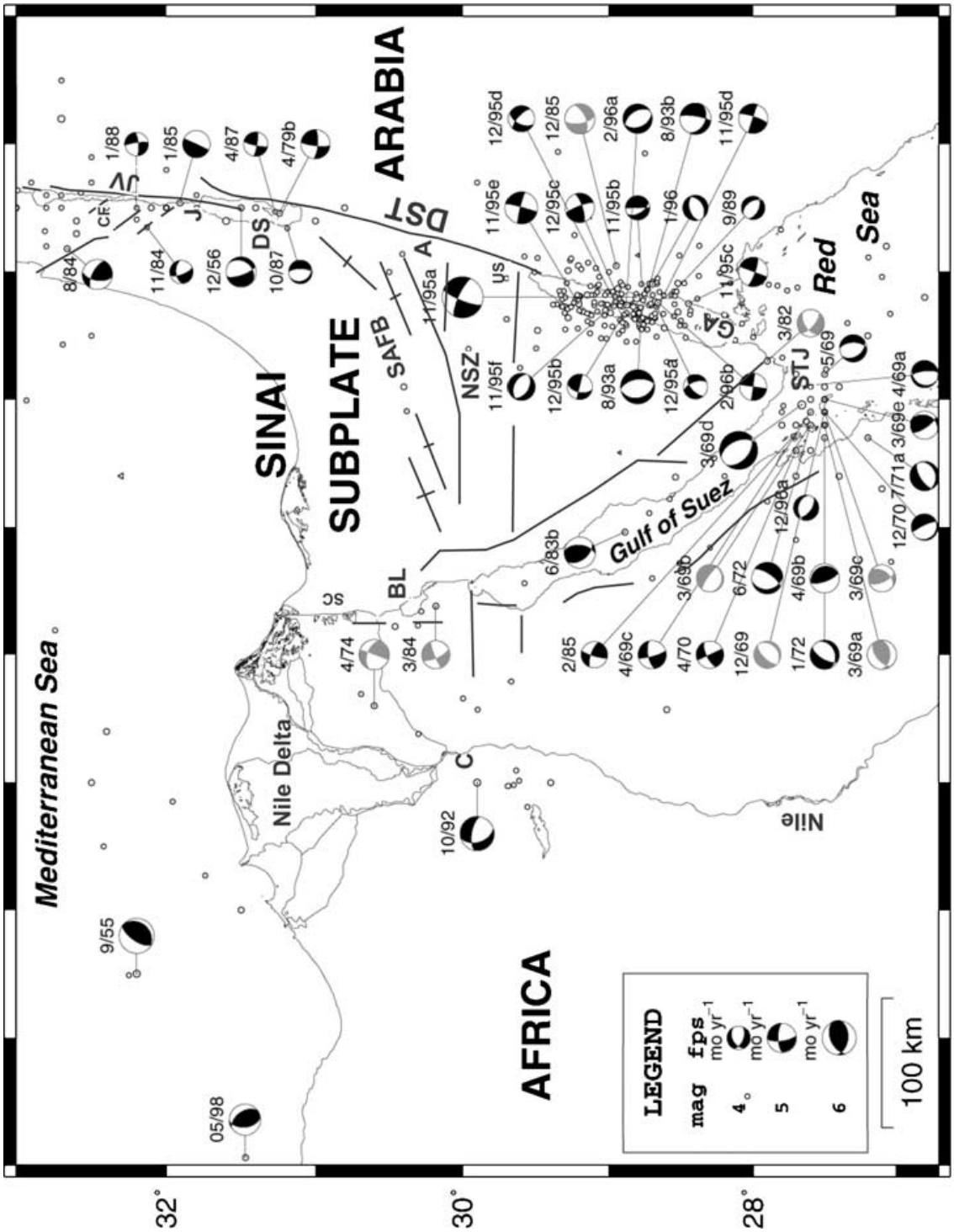

Figure 6. Seismotectonic map of the Suez Rift. See Fig. 1 for an explanation of the symbols. Plate borders are the Suez Rift along the Gulf of Suez and the Dead Sea Transform (DST). Geological elements and localities: A, Arava Valley; BL, Bitter Lakes; C, Cairo; CF, Carmel–Faria fault system; DS, Dead Sea; GA, Gulf of Aqaba; J, Jericho; JV, Jordan Valley; NSZ, Negev Shear Zone; SAFB, Syrian Arc Fold Belt; SC, Suez Canal; STJ, Sinai Triple Junction.

mechanisms of small events at the southern part of the Gulf. Yet, here we find $M_L \geq 4$ shocks that are not supported by geophysical data. Moreover, the 6/83b thrust mechanism, which occurred in a different region of the rift, and thrust events in the southern Red Sea Rift (Hofstetter & Beyth 2003) stress the role of that recently discovered phenomenon. Garfunkel & Bartov (1977) already noticed a possible reverse fault along the eastern margins of the Suez Gulf. Later study by Knott *et al.* (1995) revealed more reverse faults that are associated with major normal faulting and located at the tip of the hanging block. They attributed the reverse faults to a process of basin inversion in the Gulf. Sharp *et al.* (2000), however, related the occurrence of these faults to geometric complexities as a result of the interrelation between normal fault growth process and synrift sedimentation. Another possible explanation could be that the thrust solutions are due to a very large stress drop during the mainshock, which might result in a stress field oriented opposite to the original one—that is the 'overshoot' mechanism suggested by Savage & Wood (1971). That 'reversed' stress field, in turn, could yield aftershock mechanisms in the opposite sense to the mainshock one. Also, a slight component of shear, if it exists in the Suez Gulf, could in a certain geometrical configuration produce trans-tension/pression mechanisms. Interestingly, Bosworth & Taviani (1996) identified breakouts around the 1969 and 1972 epicentres with scattered east–west orientations and interpreted this local deviation of the minimum horizontal stress axis as being a consequence of stress relaxation following these ruptures. All of the above reinforces the need for a detailed model supported by field or geophysical data to substantiate this.

Northwest of the Gulf of Suez, and outside the rift province, the destructive 10/92 Cairo earthquake is most important. Its extensional mechanism combined with a slight shear component, fits well with both the SR system and the E–W transverse normal faults east of Cairo. To resolve which of the two nodal planes is the preferred fault requires more evidence. It seems that the mechanisms of the 1999 December 28 sequence, northeast of Cairo, of Badawy & Abdel Fattah (2001), are consistent with our 10/92 Cairo and 3/84 solutions. It also supports Bosworth & McClay's (2001) idea of a northward continuation of the SR following the same pattern as during the Miocene, via a regional left-stepping relay in the subsurface, beneath the Nile Delta. Northwards, the base of the Nile cone is crossed by a system of linear diapirs that trends to the NNW. Garfunkel & Almagor (1987) suggested that faults could trigger the growth of these diapirs and cause their linear shape. If so, these structures may be tectonically controlled by faults off the Suez Rift.

West of the Bitter Lakes and the Suez Canal, we find the interesting 4/74 and 3/84 (doubtful) shear mechanisms (Fig. 6). Both the solutions consist of nodal planes where the general E–W strikes are parallel to the fault pattern there, but with the opposite sense of motion.

The strong 9/55 earthquake and the 5/98 event just northwest of the Nile Delta show compression (Fig. 6). Ben-Avraham & Nur (1986) associated 9/55 with the convergence of Africa and Eurasia. They suggested that stresses accumulate around the Anaximander and the Eratosthenes Seamounts, rejuvenate nearby weakness zones such as the passive margins of North Africa, but with a reverse sense of motion. Event 5/98A seems to support their model as well.

Strike directions of nodal planes of mechanisms along the SR concentrate along the NNW–SSE directions (Fig. 3f). These modes are parallel to the rift axis, although some of the mechanism strikes are poorly constrained. The secondary modes reflect the other shear and thrust mechanisms.

Rake directions show the mode of normal faulting with a slight (expected?) sinistral or dextral (auxiliary?) shear component. Yet the most interesting outcome of this diagram is the presence of reverse (even though secondary) modes (Fig. 4f).

3.4 Intraplate seismicity

Intraplate activity reveals seismogenic structures outside the plate boundary zones. Unfortunately, reliable solutions of $M_L \geq 4$ intraplate events could not be obtained here, thus the tectonic interpretation could only be based solely on mechanisms of lower-magnitude events and on the pattern of seismicity (Salamon *et al.* 1996). Of great importance is the $M_L = 4.6$ earthquake of 1984 April 6, located in the central Sinai Peninsula (Negev Shear Zone—NSZ in Fig. 1). The few first-motion records (IPRG seismograms archive) do not contradict the typical right-lateral faulting of the NSZ (Bartov 1974).

The NSZ is part of the Syrian Arc belt (Krenkel 1924) that extends northeastward, across the DST, into the Arabian plate, where it is known as the Palmyrides. The Palmyrides are at least partly seismically active, as is evident from the 10/70 thrust and the 12/96 shear mechanisms (Fig. 2). Both the mechanisms seem to reflect the convergence process of Arabia towards Anatolia, in accordance with the Chaimov *et al.* (1990) and Barazangi *et al.* (1993) models. We also found the 3/89 thrust to be similar to the 10/70 solution, (Fig. 2). However, this thrust is located in Wadi Sirhan, which is a prominent morphological feature (seen on aerial photographs) that trends parallel to the Red Sea, but the Red Sea is clearly a divergent zone.

3.5 Stress inversion

Projection of P and T axes on an equal-area stereonet did not yield any significant trend (Salamon 1993). In addition, we examined the stress field along the plate boundaries using the 'stress inversion' algorithm of Reches (1987, 1990). Unfortunately, the calculations yielded high values of average misfit ($>40^\circ$) between the optimal stress tensor and the direction of maximum resolved shear stress on the fault planes, which was achieved with a very low friction coefficient of 0–0.1 (detailed results in Salamon 1993). These are unrealistic conditions that led us to conclude that the group of mechanisms is heterogeneous and reflects spatial changes in the stress fields along each of the plate borders. The problem is clearly demonstrated in the Suez Rift, where we find the normal 3/69d mechanism close to the thrust of the 6/83b event. Badawy & Horvath (1999) suggest that the Sinai subplate region is subject to a strike-slip stress regime, but note that 42 per cent of their focal solutions data set is not of the strike-slip type.

4 SYNTHESIS AND CONCLUSIONS

The slow rate of motion and low seismic efficiency, as expressed by the long repeat time of strong events (Rotstein 1987), allow us only a qualitative examination of the seismotectonics of the Sinai subplate. We therefore made a considerable effort to gather all available data and carefully scrutinize the results of our findings.

4.1 The Dead Sea Transform

The DST is characterized by a left-lateral motion and is accompanied by extension normal to it (Fig. 4a). The activity (Fig. 1) is diffused

in the region north of the Carmel-Fari'a fault system and around the Yammouneh restraining bend, but further south it is concentrated close to the rhomb-shaped pull-apart basins of the Dead Sea and the Gulf of Aqaba. This supports the idea that the lithospheric breakup and the oblique extension along the southern part of the transform occur by necking of a work-hardening plastic plate, as suggested by Agnon & Eidelman (1991).

Compared with the Alpine and the San Andreas transforms (Scholz 1990, and references therein), we find that the DST is less seismogenic, has the lowest seismic efficiency, is accompanied by the least distributed deformation and has the longest repeat time of major events. The restraining bends in these three transforms are associated with intense deformation and diffused seismicity.

4.2 The Cypriot Arc

This is the first time that the arcuate pattern of the CA has been recognized through the strike of the fault plane solutions (Fig. 5), and, as previously found, the convergent nature of the arc is clearly exhibited by thrust solutions of the greater events (Fig. 4e). Focal mechanisms in the eastern part of the arc support Kempler & Garfunkel's (1991) model and Vidal *et al.*'s (2000b) findings of left-lateral transtensional and transpressional motion between Africa (Sinai) and Anatolia.

Compared with the Hellenic Arc and the Aegean Sea, the CA is less active and lower in seismic efficiency (Jackson & McKenzie 1988). Although it is a convergent zone, it lacks the typical characteristics of subduction zones. We were not able to identify the descending slab nor the Benioff zone, and earthquakes are not deeper than 150 km, though clearly the mechanisms of the deeper events are thrusts (9/63, 11/68, 5/82, 2/87).

4.3 The Suez Rift

In contrast to the previous conception of its aseismic nature, and in accord with extensive field evidence, our seismotectonic study unequivocally indicates the existence of current activity along the SR (Fig. 1). In general, the focal mechanisms show the expected extension across the rift, but at the same time they also reflect the complexities of its present stress field. Although not absolutely certain, it also raises the possibility of hitherto unknown structural elements (Fig. 6). Comparing the rake direction of mechanisms in SR (Fig. 4f) and the Gulf of Aqaba (Fig. 4c), it is clear that these are two different tectonic regimes.

4.4 The intraplate zone

Being a small region comprised of heterogeneous crustal structure (Ginzburg *et al.* 1979) and surrounded by active boundaries that induce a heterogeneous stress field, this area produces some activity, though its nature is yet to be deciphered.

4.5 The Sinai subplate

Our study which examines a century-long time span of seismotectonic activity, demonstrates primarily the relations between seismicity and earthquake mechanisms in the eastern Mediterranean and the Levant Basin regions, and its plate tectonic characteristics.

(1) The northeastern tip of the African Plate and the Levant Basin are in an ongoing process of breakup along the SR (Said 1962; Robson 1971; Ben-Menahem *et al.* 1976; Garfunkel & Bartov 1977), a process yet to be completed. We therefore define this tip as a distinct component in the plate tectonics of the eastern Mediterranean region, and term it the Sinai subplate.

(2) Most of the seismicity and the seismic moment are concentrated and released within a seismogenic belt that stretches along the DST, the CA and the SR (Fig. 1). They also reflect the sense of relative motion along the plate boundaries. Yet north of the SR the seismic activity disperses and terminates, showing that the area is still connected to the African Plate. These findings support the conclusions of Ben-Menahem *et al.* (1976).

(3) Some of the focal mechanisms suggest a complex relationship between the deformation of the plate boundaries and the relative plate motions. These include the enigmatic thrusts in the Gulf of Suez (Fig. 6), the shear between the Eratosthenes Seamount and the CA (Fig. 5), and transpression on, or near, the Carmel Fault (Fig. 2). These phenomena require further investigation in order to clarify in more detail how the ongoing deformation of the Sinai subplate in these regions is related to the plate motions.

(4) The distribution of nodal plane strikes (Fig. 3) coincides with the azimuth of the plate borders, and the distribution of rake directions (Fig. 4) reflects the sense of motion and style of deformation between neighbouring plates.

Overall, within the global framework of plate tectonics, the Sinai subplate is hardly distinguished, for its seismicity, volcanism and topography are only of secondary magnitude. However, by studying the seismotectonics of the eastern Mediterranean region, we were able to establish the grounds on which to recognize the Sinai subplate as a significant component in the role of the Levant Plate tectonics.

ACKNOWLEDGMENTS

We are greatly indebted to Dr Avi Shapira for his generous support of this work, which was carried out within the framework of the seismological division of the Geophysical Institute of Israel (GII). Fruitful discussions with him and with Drs T. van Eck, A. Agnon, Y. Rotstein, Y. Bartov, N. Rabinowitz, D. Kempler and G. Shamir were very helpful and are greatly appreciated. A critical review by W. Bosworth and T. Taymaz helped us to revise and improve our work.

The generous assistance of Ms Batia Reich, Lea Feldman, Corinne Ben-Sasson, Veronic Avirav and the technical crew of the GII are appreciatively acknowledged. Figures in this study were created using the 'GMT' plotting procedure (Wessel & Smith 1991) and the 'GEOrient' structural geology software (Holcombe 2001). AS thanks Berkeley Seismographic Station and Dr G. Baer for their help in preparing the seismotectonic maps, and Mrs B. Katz for help with editing the English manuscript. This study was part of AS's doctoral thesis, carried out at The Hebrew University of Jerusalem and at the Geophysical Institute of Israel. He also wishes to thank the Faculty Development Programme of the Institute of Earth Sciences (The Friedman Fellowship) at The Hebrew University, for its support.

REFERENCES

Achmon, M. & Ben-Avraham, Z., 1997. The deep structure of the Carmel fault zone, northern Israel, from gravity field analysis, *Tectonics,* **16,** 563–569.

Agnon, A., 1981. Neogene development of the western margin of the southern Dead Sea depression, *Isr. Geol. Surv., Current Res.*, 27–29.

Agnon, A. & Eidelman, A., 1991. Lithospheric breakup in three dimensions: necking of a work-hardening plastic plate, *J. geophys. Res.,* **96,** 20 189–20 194.

Alamari, A.M., Scholt, F.R. & Bufe, C.G., 1991. Seismicity and aeromagnetic features of the Gulf of Aqaba (Elat) region, *J. geophys. Res.,* **96,** 20 179–20 185.

Ambraseys, N.N. & Adams, R.D., 1993. Seismicity of the Cyprus region, *Terra Nova,* **5,** 85–94.

Amit, R., Zilberman, E., Porat, N. & Enzel, Y., 1999. Relief inversion in the Avrona Playa as evidence of large-magnitude historical earthquakes, Southern Arava Valley, Dead Sea Rift, *Quat. Res.,* **52,** 76–91.

Arieh, E., Rotstein, Y. & Peled, U., 1982. The Dead Sea earthquake of 23 April 1979, *Bull. seism. Soc. Am.,* **72,** 1627–1634.

Avni, Y., Bartov, Y., Garfunkel, Z. & Ginat, H., 2000. Evolution of the Paran drainage basin and its relation to the Plio-Pleistocene history of the Arava Rift western margin, Israel, *Isr. J. Earth Sci.,* **49,** 215–238.

Badawy, A., 2001. Status of the crustal stress in Egypt as inferred from earthquake focal mechanisms and borehole breakouts, *Tectonophysics,* **343,** 49–61.

Badawy, A. & Abdel Fattah, A.K., 2001. Source parameters and fault plane determinations of the 28 December 1999 northeastern Cairo earthquakes, *Tectonophysics,* **343,** 63–77.

Badawy, A. & Horvath, F., 1999. Recent stress field of the Sinai subplate region, *Tectonophysics,* **304,** 385–403.

Barazangi, M., Seber, D., Chaimov, T., Best, J., Litak, R., Al-Saad, A. & Sawaf, T., 1993. Tectonic evolution of the northern Arabian plate in western Syria, in *Recent Evolution and Seismicity of the Mediterranean Region,* pp. 117–140, eds Boschi, E., Mantovani, E. & Morelli, A., Kluwer Academic Publishers, the Netherlands.

Bartov, J., 1974. A structural and paleogeographical study of the central Sinai faults and domes, *PhD thesis*, Hebrew University of Jerusalem (in Hebrew with English abstract).

Ben-Avraham, Z. & Ginzburg, A., 1990. Displaced terranes and crustal evolution of the Levant and the Eastern Mediterranean, *Tectonics,* **9,** 613–622.

Ben-Avraham, Z. & Nur, A., 1986. Collisional processes in the Mediterranean, *Geolog. Rund.,* **75/1,** 209–217.

Ben-Avraham, Z. & Zoback, M.D., 1992. Transform-normal extension and asymmetric basins: an alternative to pull-apart models, *Geology,* **20,** 423–426.

Ben-Avraham, Z., Garfunkel, Z., Almagor, G. & Hall, J.K., 1979. Continental breakup by a leaky transform: the Gulf of Elat (Aqaba), *Science,* **206,** 214–216.

Ben-Menahem, A. & Aboodi, E., 1971. Tectonic patterns in the Red Sea region, *J. geophys. Res.,* **76,** 2674–2689.

Ben-Menahem, A., Nur, A. & Vered, M., 1976. Tectonics, seismicity and structure of the Afro-Euroasian junction—the breaking of an incoherent plate, *Phys. Earth planet. Inter.,* **12,** 1–50.

Bosworth, W. & McClay, K., 2001. Structural and stratigraphic evolution of the Gulf of Suez rift, Egypt: a synthesis, in *Peri-Tethys Memoir 6: Peri-Tethyan rift/wrench basins and passive margins. Memoires du Museum National d'Histoire Naturalle de Paris,* Vol. 186, pp. 567–606, eds Ziegler, P.A., Cavazza, W., Robertson, A.H.F. & Crasquin-Soleau, S.

Bosworth, W. & Strecker, M.R., 1997. Stress field changes in the Afro-Arabian rift system during the Miocene to recent period, in *Structure and Dynamic Processes in the Lithosphere of the Afro-Arabian Rift System, Tectonophysics,* Vol. 278, pp. 47–62, eds Fuchs, K., Altherr, R., Mueller, B. & Prodehl, C.

Bosworth, W. & Taviani, M., 1996. Late Quaternary reorientation of stress field and extension direction in the southern Gulf of Suez, Egypt: Evidence from uplifted coral terraces, mesoscopic fault arrays, and borehole breakouts, *Tectonics,* **15,** 791–802.

Buyukasikoglu, S., 1980. Euroasian–African plate boundary in southern Turkey and Eastern Mediterranean, *Proceed. 7th World Conf. Earthquake Engin., Istanbul,* **1,** 209–212.

Canitez, N. & Ucer, S., 1967. Computer determinations for the fault plane solutions in and near Anatolia, *Tectonophysics,* **4,** 235–244.

Chaimov, T.A., Barazangi, M., Al-Saad, D., Sawaf, T. & Gebran, A., 1990. Crustal shortening in the Palmyride fold belt, Syria, and implications for movement along the Dead Sea fault system, *Tectonics,* **9,** 1369–1386.

Constantinescu, L., Ruprechtova, L. & Enescu, D., 1966. Mediterranean-Alpine earthquake mechanisms and their seismo-tectonic implications, *Geophys. J. R. astr. Soc.,* **10,** 347–368.

De-Sitter, L.U., 1962. Structural development of the Arabian shield in Palestine, *Geol. en. Mijnb.,* **45,** 116–124.

Deschamps, A. & King, G.C.P., 1984. Aftershocks of the Campania-Lucania (Italy) earthquake of 23 November 1980, *Bull. seism. Soc. Am.,* **74,** 2483–2517.

Dewey, J.F., Pitman, W.C., Ryan, W.B.F. & Bonnin, J., 1973. Plate tectonics and the evolution of the Alpine system, *Bull. Geol. Soc. Am.,* **84,** 3137–3180.

Drakopoulos, J. & Delibasis, N., 1982. *The Focal Mechanism of Earthquakes in the Major Area of Greece for the period 1947–1981*, Univ. of Athens, Seismol. Lab.

Ellenblum, R., Marco, S., Agnon, A., Rockwell, T. & Boas, A., 1998. Crusader castle torn apart by earthquake at dawn, 20 May 1202, *Geology,* **26,** 303–306.

Freund, R., 1965. A model of the structural development of Israel and adjacent areas since upper Cretaceous times, *Geol. Mag.,* **102,** 189–205.

Freund, R., Garfunkel, Z., Zak, I., Goldberg, M., Weissbrod, T. & Derin, B., 1970. The shear along the Dead Sea Rift, *Phil. Trans. R. Soc. Lond.*, A, **267,** 107–130.

Gardosh, M., Reches, Z. & Garfunkel, Z., 1990. Holocene tectonic deformation along the western margins of the Dead Sea, *Tectonophysics,* **180,** 123–137.

Garfunkel, Z., 1981. Internal structure of the Dead Sea leaky transform (rift) in relation to plate kinematics, *Tectonophysics,* **80,** 81–108.

Garfunkel, Z., 1998. Constrains on the origin and history of the Eastern Mediterranean basin, *Tectonophysics,* **298,** 5–35.

Garfunkel, Z. & Almagor, G., 1987. Active salt dome development in the Levant basin, southeast mediterranean, in *Dynamical Geology of Salt and Related Structures,* pp. 263–300, eds Lerche, I. & O'brien, J., Academic Press, London.

Garfunkel, Z. & Bartov, Y., 1977. The tectonics of the Suez Rift, *Israel Geol. Surv. Bull.,* **71,** 44.

Garfunkel, Z. & Ben-Avraham, Z., 2001. Basins along the Dead Sea transform, in *Peri-Tethys Memoir 6: Peri-Tethyan Rift/Wrench Basins and Passive Margins,* Vol. 186, pp. 607–627, eds Ziegler, P.A., Cavazza. W., Robertson, A.H.F. & Crasquin-Soleau, S., Mem. du Musee Nat. d'Hist. naturell, Paris.

Garfunkel, Z. & Derin, B., 1985. Permian–Early Mesozoic tectonism and continental margin formation in Israel and its implications for the history of the Eastern Mediterranean, in *The Geological Evolution of the Eastern Mediterranean,* pp. 187–201, eds Dixon, J.E. & Robertson, A.H.F. Special Publication of the Geological Society No. 17, Blackwell, Oxford.

Garfunkel, Z., Zak, Y. & Freund, R., 1981. Active faulting in the Dead Sea rift, *Tectonophysics,* **80,** 1–26.

GII, 1996. *Seismological Bulletin 1900–1995,* Seismology Division, Geophy. Inst. Isr. http://www.gii.co.il/

Ginzburg, A., Makris, J., Fuchs, K., Prodhel, C., Kaminski, W. & Amitai, U., 1979. A seismic study of the crust and upper-mantle of the Jordan-Dead Sea rift and their transition toward the Mediterranean sea, *J. geophys. Res.,* **84,** 1569–1582.

Glover, C. & Robertson, A., 1998. Neotectonic intersection of the Aegean and Cyprus tectonic arcs: extensional and strike-slip faulting in the Isparta Angle, SW Turkey, *Tectonophysics,* **298,** 103–132.

Gomez, F., Meghraoui, M., Darkal, A.N., Sbeinati, R., Darawcheh, R., Tabet, C., Knawlie, M., Charabe, M., Khair, K. & Barazangi, M., 2001. Coseismic displacements along the Serghaya Fault: an active branch of the Dead Sea Fault System in Syria and Lebanon, *J. geol. Soc. Lond.,* **158,** 405–408.

Hall, J.K., 1994. Bathimetric chart of the Eastern Mediterranean, *Isr. Geol. Surv.,* 1 Map, Scale 1:625 000. Plate 1 (Fig. 1.13), in eds Hall, J.K., Udinstev, G.B. & Odinokov, Yu.Yu. 1994. The bottom relief of the Levantine Sea, in *Geological Structure of the North-Eastern Mediterranean,*

(Cruise 5 of the Research Vessel 'Akademik Nikolaj Strakhov'), eds Krasheninnikov, V.A. & Hall, J.K., Historical Productions-Hall, Jerusalem, pp. 5–32.

Hancock, P.L. & Atiya, M.S., 1979. Tectonic significance of mesofracture systems associated with the Lebanese segment of the Dead Sea transform fault, *J. Struct. Geol.,* **1,** 143–153.

Hatzfeld, D., Christodoulou, A.A., Scordilis, E.M., Panagiotopoulos, D. & Hatzidimitriou, P.M., 1986. A microearthquake study of the Mygdonian graben (northern Greece), *Earth planet. Sci. Lett.,* **81,** 379–396.

Hauksson, E. & Jones, L.M., 1989. The 1987 Whittier Narrows earthquake sequence in Los Angeles, southern California: seismological and tectonic analysis, *J. geophys. Res.,* **94,** 9569–9589.

Hodgeson, J.H. & Adams, W.M., 1958. A study of inconsistent observations in the fault plane project, *Bull. seism. Soc. Am.,* **48,** 17–31.

Hofstetter, R. & Beyth, M., 2003. The Afar depression: Interpertation of the 1960–2000 earthquakes, *Geophys. J. Int.,* in press.

Hofstetter, A., van Eck, T. & Shapira, A., 1996. Seismic activity along fault branch of the Dead Sea–Jordan Transform System: the Carmel–Tirtza fault system, *Tectonophysics,* **267,** 317–330.

Hofstetter, A., Thio, H.K. & Shamir, G., 2003. Source mechanisms of the 22/11/1995 Gulf of Aqaba earthquake and its aftershock sequence, *J. Seism.,* **7,** 99–114.

Holcombe, R.J., 2001. GEOrient 8.0, Structural Geology Software, http://www.earthsciences.uq.edu.au/∼rodh/software.

Horowitz, A., 2001. The Jordan Rift Valley, A.A., p. Vol. 730, Balkema, Lisse.

Huang, P.Y. & Solomon, S.C., 1987. Centroid depth and mechanisms of mid-ocean ridge earthquakes in the Indian Ocean, Gulf of Aden and Red Sea, *J. geophys. Res.,* **92,** 1361–1382.

Hurukawa, N. *et al.*, 2001. Seismological observations in and around the southern part of the Gulf of Suez, Egypt, *Bull. seism. Soc. Am.,* **91,** 708–717.

IPRG Seismological Bulletins, 1–12,1982–1993. *Earthquakes in and around Israel,* Seismological Division, Inst. Petrol. Res. Geophys., Holon, Israel. http://www.gii.co.il/.

ISC, 1964–1993. *Bulletin of the International Seismological Centre,* Edinburgh.

ISC Bulletin Data Base, 1991. *FAISE Retrieval Software for the Hypocenter Associated Data CD-ROM*, USGS/NEIC.

ISC, 2000. *Database Selection,* http://www.isc.ac.uk/Bulletin/index˙db.html

ISS, 1918–1963. *Bulletin of the International Seismological Summary,* Berkshire, UK.

Jackson, J., 1992. Partitioning of strike slip and convergent motion between Euroasia and Arabia in Turkey and the Caucasus, *J. geophys. Res.,* **97,** 12 471–12 479.

Jackson, J. & McKenzie, D., 1988. The relationship between plate motions and moment tensors, and the rates of active deformation in the Mediterranean and Middle East, *Geophys. J. Int.,* **93,** 45–73.

Jackson, J.A., White, N.J., Garfunkel, Z. & Anderson, H., 1988. Relations between normal-fault geometry, tilting and vertical motions in extensional terrains: an example from the southern Gulf of Suez, *J. Struct. Geol.,* **10,** 155–170.

Joffe, S. & Garfunkel, Z., 1987. Plate kinematics of the Circum Red Sea—a re-evaluation, *Tectonophysics,* **141,** 5–22.

JSO, 1984–1993. *Seismological Bulletins 2–24*. *Earthquakes in Jordan and adjacent areas*. Seismol. Div., Jordan Seismol. Obs., Amman, Jordan.

Karcz, Y., 1959. The structure of the northern Carmel, *Isr. Res. Council,* **8G,** 119–130.

Kempler, D., 1994. An outline of North-Eastern Mediterranean tectonics in view of Cruise 5 of the Akademik Nikolaj Strakhov, in *Geological Structure of the North-Eastern Mediterranean (Cruise 5 of the Research Vessel 'Akademik Nikolaj Strakhov'* pp. 277–293, Krasheninnikov, V.A. & Hall, J.K., Historical Productions-Hall, Jerusalem.

Kempler, D. & Ben-Avraham, Z., 1987. The tectonic evolution of the Cyprean arc, *Ann. Tectonicae,* **1,** 58–71.

Kempler, D. & Garfunkel, Z., 1991. The northeast Mediterranean triple junction from a plate kinematics point of view, *Bull. Tech. Univ. Istanbul,* **44,** 203–232.

Klinger, Y., Avouac, J.P., Abou Karaki, N., Dorbath, L., Bourles, D. & Reyss, J.L., 2000a. Slip rate on the Dead Sea transform in northern Araba valley (Jordan), *Geophys. J. Int.,* **142,** 755–768.

Klinger, Y., Avouac, J.P., Dorbath, L., Abou Karaki, N. & Tisnerat, N., 2000b. Seismic behaviour of the Dead Sea fault along Araba valley, Jordan, *Geophys. J. Int.,* **142,** 769–782.

Klinger, Y, Rivera, L., Haessler, H. & Maurin, J.C., 1999. Active faulting in the Gulf of Aqaba: new knowledge from the M_W 7.3 earthquake of 22 November 1995, *Bull. seism. Soc. Am.,* **89,** 1025–1036.

Knott, S.D., Beach, A., Welbon, A.I. & Brockbank, P.J., 1995. Basin inversion in the Gulf of Suez: implications for exploration and development in failed rifts, in *Basin Inversions, Geol. Soc. London, Spec. Publ.,* Vol. 88, pp. 59–81 Buchanan, J.G. & Buchanan, P.G.

Kovach, R.L., Andreasen, G.E., Gettings, M.E. & El-Kayasi, K., 1990. Geophysical investigations in Jordan, *Tectonophysics,* **180,** 61–69.

Krenkel, E., 1924. Der Syrische Bogen, *Centralblatt für Mineralogie, Geologie und Palaontologie,* pp. 274–281.

Larson, E., 1999. *Harvard Seismology CMT Catalog Search*, http://www.seismology.harvard.edu/CMTsearch.html.

Le Pichon, X. & Francheteau, J., 1978. A plate-tectonic analysis of the Red Sea–Gulf of Aden area, *Tectonophysics,* **46,** 369–406.

Lyberis, N., 1988. Tectonic evolution of the Gulf of Suez and The Gulf of Aqaba, *Tectonophysics,* **153,** 209–220.

Lyberis, N., Yurur, T., Chorowicz, J., Kasapoglu, E. & Gundogdu, N., 1992. The east Anatolian fault: an oblique collisional belt, *Tectonophysics,* **204,** 1–15.

Lyon-Caen, H. *et al.*, 1988. The 1986 Kalamata (south Peloponesus) earthquake: detailed study of a normal fault, evidence for east–west extension in the Hellenic arc, *J. geophys. Res.,* **93,** 14 967–15 000.

Marco, S., Agnon, A., Ellenblum, R., Eidekman, A., Basson, U. & Boas, A., 1997. 817-year-old walls offset sinistrally 2.1 m by the Dead Sea transform, Israel, *J. Geodyn.,* **24,** 11–20.

Marco, S., Heimann, A., Rockwell, K.T. & Agnon, A., 2000. Late Holocene earthquake deformations in the Jordan Gorge Fault, Dead Sea Transform in *Abstracts of Isr. Geol. Soc., Annu. Meet. Ma'alot,*, p. 85, Israel geological Society, Jerusalem.

Mart, Y., 1991. The Dead Sea Rift: from continental rift to incipient ocean, *Tectonophysics,* **197,** 155–179.

Mascle, J., Benkhelil, J., Bellaiche, G., Zitter, T., Woodside, J., Loncke, L. & Prismed II Scientific Party, 2000. Marine geologic evidence for a Levantine–Sinai Plate, a new piece of the Mediterranean puzzle, *Geology,* **28,** 779–782.

McKenzie, D.P., 1970. Plate tectonics of the Mediterranean region, *Nature,* **226,** 239–243.

McKenzie, D., 1972. Active tectonics of the Mediterranean region, *Geophys. J. R. astr. Soc.,* **30,** 109–185.

McKenzie, D., 1976. The east Anatolian fault: A major structure in eastern Turkey, *Earth planet. Sci. Lett.,* **29,** 189–193.

McKenzie, D.P., Davies, D. & Molnar, P., 1970. Plate tectonics of the Red Sea and East Africa, *Nature,* **226,** 243–248.

Mor, U., 1987. The geology of the Judean Desert in the area of Nahal Darga, *MSc thesis*, The Hebrew University of Jerusalem (in Hebrew).

Niemi, T.M., 1997. Preliminary estimate of paleoearthquakes along the northern Wadi Araba Fault, Dead Sea Transform, Jordan, *GSA Abtracts with Programs*, **29,** A-131.

Oppenheimer D.H., Reasenberg, P.A. & Simpson, R.W., 1988. Fault plane solutions for the 1984 Morgan Hill, California, earthquake sequence: evidence for the state of stress on the Calaveras fault, *J. geophys. Res.,* **93,** 9007–9026.

Papazachos, B.C. & Papaioannov, Ch.A., 1999. Lithospheric boundaries and plate motions in the cyprus area, *Tectonophysics,* **308,** 193–204.

Patton, T.L., Moustafa, A.R., Nelson, R.A. & Abdine, S.A., 1994. Tectonic evolution and structural setting of the Suez Rift, in *Interior Rift Basins, Am. Ass. Petrol. Geol. Mem.,* Vol. 59, pp. 7–55, ed. Landon, S.M.

Perincek, D. & Cemen, I., 1990. The structural relationship between the East Anatolian and Dead Sea fault zones in southeastern Turkey, *Tectonophysics,* **172,** 331–340.

Pho, H.T. & Behe, L., 1972. Extended distance and angles of incidence of *P* waves, *Bull. seism. Soc. Am.,* **62,** 885–902.
Pinar, A. & Kalafat, D., 1999. Source processes and seismotectonic implications of the 1995 and 1996 Cyprus, Eastern Mediterranean region, earthquakes, *Tectonophysics,* **301,** 217–230.
Pinar, A. & Turkelli, N., 1997. Source inversion of the 1993 and 1995 Gulf of Aqaba earthquakes, *Tectonophysics,* **283,** 279–288.
Quennell, A.M., 1959. Tectonics of the Dead Sea Rift, *Int. Geol. Congr., Mexico,* 385–405.
Raz, E., 1983. *The Geology of the Judean Desert—'En Gedi Area,* Isr. Geol. Surv. Rep., S/3/83 (in Hebrew).
Reasenberg, P. & Oppenheimer, D., 1985. *FPFIT, FPPLOT and FPPAGE: Fortran Computer Programs for Calculating and Displaying Earthquake Fault-plane Solutions,* USGS, Open-file report 85–739.
Reches, Z., 1987. Determination of the tectonic stress tensor from slip along faults that obey the Coulomb yield condition, *Tectonics,* **6,** 849–861.
Reches, Z., 1990. *Stress Inversion of Fault Slip Data and Focal Plane Solutions*, A program for IBM-PC, Version 2.5.
Reches, Z. & Hoexter, D.F., 1981. Holocene seismic activity in the Dead Sea area, *Tectonophysics,* **80,** 235–254.
Ritsema, A.R., 1974. *The Earthquake Mechanisms of the Balkan Region*, Koninklijk Nederlands Meteorologisch Institut.
Robertson, A.H.F., 1998. Tectonic significance of the Eratosthenes Seamount: a continental fragment in the process of collision with a subduction zone in the eastern Mediterranean (Ocean Drilling Program Leg 160), *Tectonophysics,* **298,** 63–82.
Robertson, A.H.F., Eaton, S., Follows, E.J. & McCallum, J.E., 1991. The role of local tectonics versus global sea-level change in the Neogene evolution of the Cyprus active margin, *Spec. Pub. Int. Assoc. Sediment.,* **12,** 331–369.
Robson, D.A., 1971. The structure of the Gulf of Suez (Clysmic) rift, with special reference to the eastern side, *J. Geol. Soc. London,* **127,** 247–276.
Rojay, B., Heimann, A. & Toprak, V., 2001. Neotectonic and volcanic characteristics of the Karasu fault zone (Anatolia, Turkey): the transition zone between the Dead Sea transform and the East Anatolian fault zone, *Geodinamica Acta,* **14,** 197–212.
Ron, H. & Eyal, Y., 1985. Intraplate deformation by block rotation and mesostructures along the Dead Sea transform, northern Israel, *Tectonics,* **4,** 85–105.
Ron, H., Nur, A. & Hofstetter, A., 1990. Late Cenozoic and recent strike slip tectonics in Mt Carmel, Northern Israel, *Ann. Tectonicae,* **4,** 70–80.
Rotstein, Y., 1987. Gaussian probability estimate for large earthquake occurrence in the Jordan Valley, Dead Sea rift, *Tectonophysics,* **141,** 95–105.
Rotstein, Y., Bartov, Y. & Hofstetter, A., 1991. Active compressional tectonics in the Jericho area, Dead Sea Rift, *Tectonophysics,* **198,** 239–259.
Rotstein, Y., Bruner, I. & Kafri, U., 1993. High resolution seismic imaging of the Carmel fault and its implications to the structure of Mt Carmel, *Isr. J. Earth Sci.,* **42,** 55–69.
Rotstein, Y. & Kafka, A.L., 1982. Seismotectonics of the southern boundary of Anatolia, Eastern Mediterranean region: subduction, collision and arc jumping, *J. geophys. Res.,* **87,** 7694–7706.
Said, R., 1962. *The Geology of Egypt,* Elsevier, p. 377.
Salamon, A., 1993. Seismotectonic analysis of earthquakes in Israel and adjacent areas, *PhD thesis,* Hebrew University of Jerusalem (in Hebrew with English abstract).
Salamon, A., Hofstetter, A., Garfunkel, Z. & Ron, H., 1996. Seismicity of the eastern Mediterranean region: perspective from the Sinai subplate, *Tectonophysics,* **263,** 293–305.
Savage, J.C. & Wood, M.D., 1971. The relation between apparent stress and stress drop, *Bull. seism. Soc. Am.,* **61,** 1381–1388.
Scholz, H.C., 1990. *The Mechanics of Earthquakes and Faulting*, p. 439, Cambridge University Press, Cambridge.
Shaliv, G., 1972. Hydrogeology of the Nahal Phari'a area, *MSc thesis*, School for Applied Sciences, Hebrew University of Jerusalem.
Shamir, G., Baer, G. & Hofstetter, A., 2003. Three-dimensional Elastic earthquake modeling based on integrated seismological and InSar data: the $M_w = 7.2$ Nuwieba earthquake, Gulf of Eilat/Aqaba, November 1995, *Geophys. J. Int.,* **154,** 731–744.
Shapira, A., 1988. Magnitude scales for regional earthquakes monitored in Israel, *Isr. J. Earth Sci.,* **37,** 17–22.
Shapira, A. & Hofstetter, A., 1993. Source parameters and scaling relationships of earthquakes in Israel, *Tectonophysics,* **217,** 217–226.
Sharp, I.R., Gawthorpe, R.L., Underhill, J.R. & Gupta, S., 2000. Fault-propagation folding in extensional settings; examples of structural style and synrift sedimentary response from the Suez Rift, Sinai, Egypt, *Geol. Soc. Am. Bull.,* **112,** 1877–1899.
Taymaz, T., Eyidogan, H. & Jackson, J., 1991. Source parameters of large earthquakes in the East Anatolian Fault Zone (Turkey), *Geophys. J. Int.,* **106,** 537–550.
Udias, A., Buforn, E. & Ruiz de Gauna, J., 1989. *Catalogue of Focal Mechanisms of European Earthquakes*, Department of Geophysics, Universidad Complutense, Madrid.
van Eck, T. & Hofstetter, A., 1989. Microearthquake activity in the Dead Sea region, *Geophys. J. Int.,* **99,** 605–620.
van Eck, T. & Hofstetter, A., 1990. Fault geometry and spatial clustering of microearthquakes along the Dead-Sea–Jordan rift fault zone, *Tectonophysics,* **180**, 1,15–27.
Vidal, N., Alvarez-Marron, J. & Klaeschen, D., 2000a. Internal configuration of the Levantine from seismic reflection data (eastern Mediterranean), *Earth planet. Sci. Lett.,* **180,** 77–89.
Vidal, N., Alvarez-Marron, J. & Klaeschen, D., 2000b. The structure of the Africa–Anatolia plate boundary in the eastern Mediterranean, *Tectonics,* **19,** 723–739.
Vidal, N., Klaeschen, D., Kopf, A., Docherty, C., von-Huene, R. & Krasheninnikov, V.A., 2000c. Seismic images at the convergence zone from south of Cyprus to the Syrian coast, eastern Mediterranean, *Tectonophysics,* **329,** 157–170.
Wessel, P. & Smith, W.H.F., 1991. Free software helps map and display data, *EOS, Trans. Am. geophys. Un.,* **72**, 441,445–446.
Wickens, J.W. & Hodgeson, J.H., 1967. *Computer Re-evaluation of Earthquake Mechanism Solutions,* Department of Energy, Mines and Resources, Ottawa.
Wilson, J.T., 1965. A new class of faults and their bearing on continental drift, *Nature,* **207,** 343–347.
Woodside, J.M., 1977. Tectonic elements and crust of the eastern Mediterranean, *Mar. Geophys.,* **3,** 317–354.
Yielding, G., Ouyed, M., King, G.C.P. & Hatzfeld, D., 1989. Active tectonics of the Algerian Atlas Mountains—evidence from aftershocks of the 1980 El Asnam earthquake, *Geophys. J. Int.,* **99,** 761–788.
Yolsal, S. & Taymaz, T., 2002. Source parameters of the Cyprean earthquakes obtained from inversion of teleseismic *P*- and *SH*-body-waveforms, *1st Int. Symp. of Istanbul Technical University the Faculty of Mines on Earth Sciences and Engineering,* 16–18May 2002, Istanbul, Turkey, Abstract Book: SS-B-Poster, p. 71.
Zhang, H. & Niemi, T.M., 1999. Slip rate of the northern Wadi Araba Fault, Dead Sea Transform, Jordan., *GSA Abstracts with Programs,* **31**, A-114.
Zilberman, E., Amit, R., Heimann, A. & Porat, N., 2000. Changes in Holocene paleoseismic activity in the Hula pull-apart basin, Dead Sea Rift, northern Israel, *Tectonophysics,* **321,** 237–252.

APPENDIX A: FOCAL SPHERES OF THE FAULT PLANE SOLUTIONS OF FIRST *P*-WAVE ARRIVALS

Focal spheres of the fault plane solutions of *P*-wave arrivals calculated in this research. Solutions are signed by origin time and presented by lower-hemisphere equal-area projection. Circles signify compressional rays (up) and triangles signify dilatational rays (down). *P* (pressure axis) denotes compressional quadrants and *T* (tension axis) tensional quadrants. '*' denotes poor quality solutions. List of solution parameters appears in Table 1, reliability of the solutions in Table 4, and notes in Appendix B.

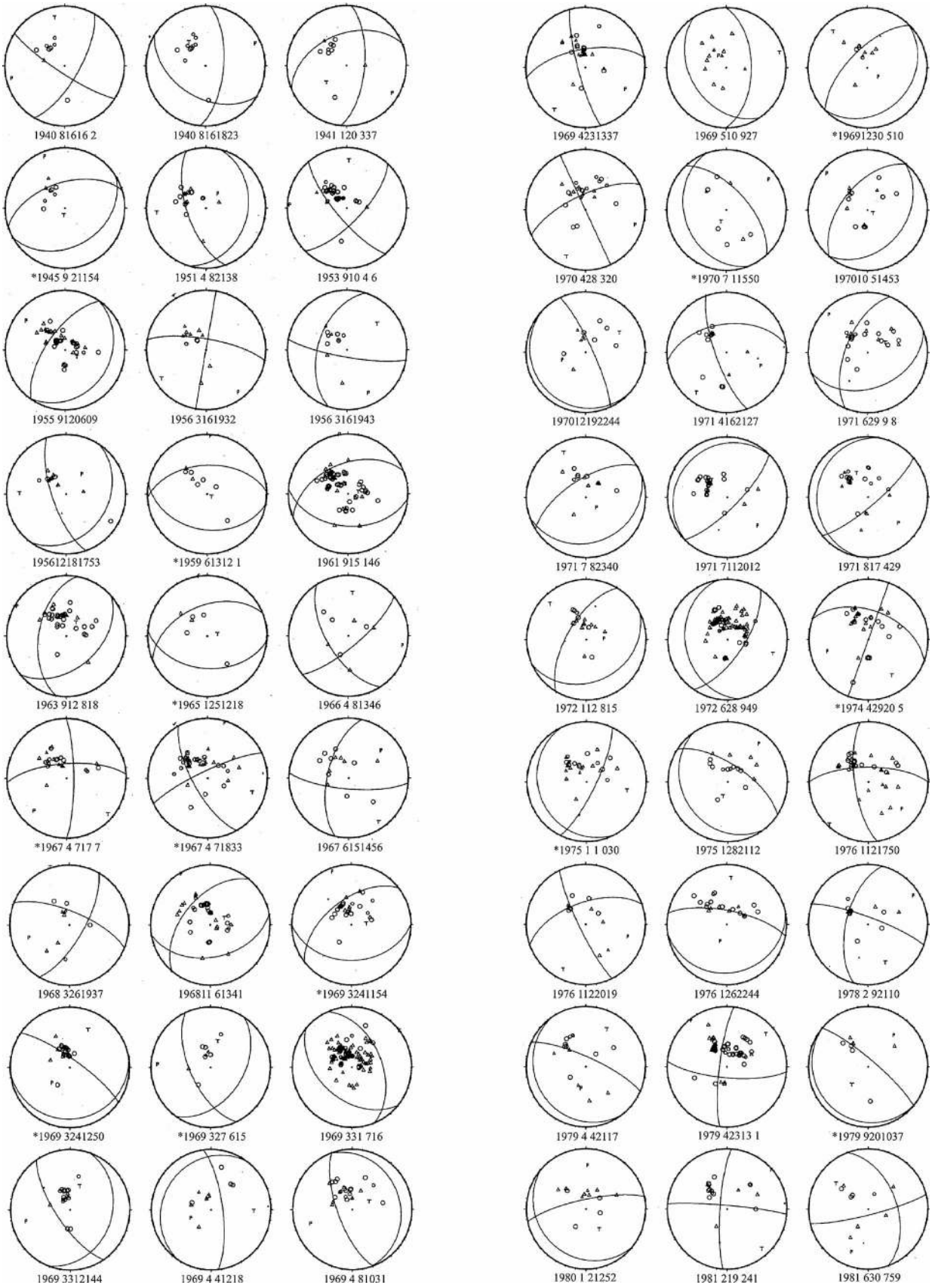

Figure A1.

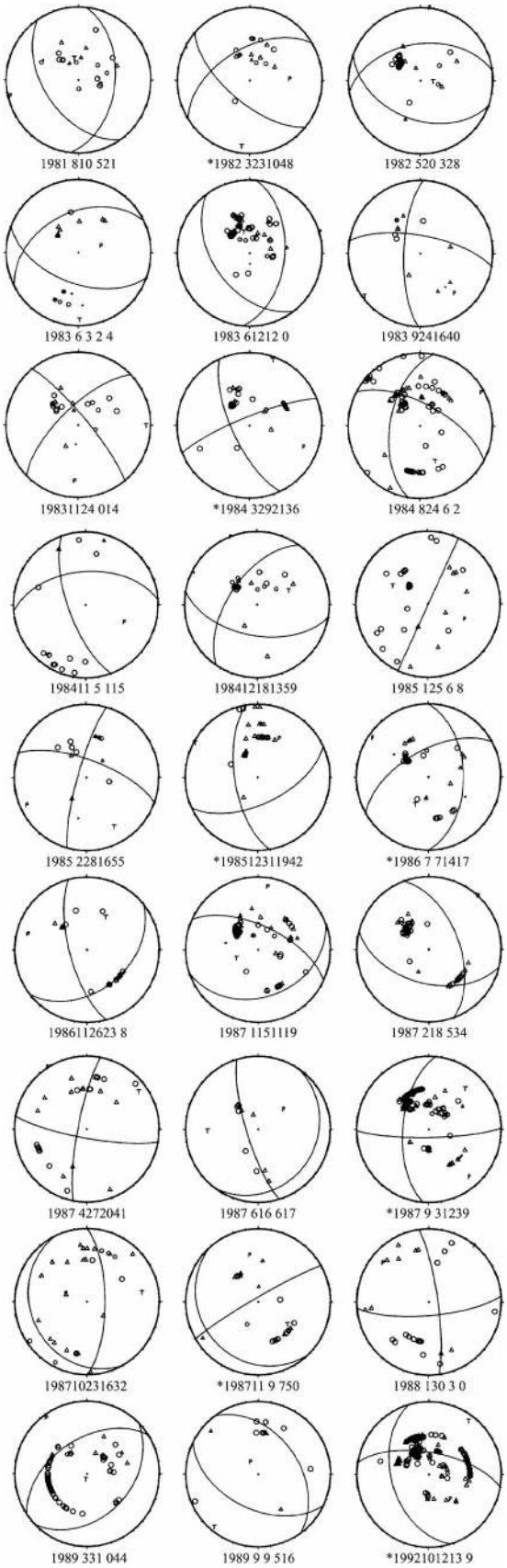

Figure A2.

APPENDIX B: NOTES REGARDING THE FAULT PLANE SOLUTIONS OF FIRST *P*-WAVE ARRIVALS

(1) 'No' is the serial number of event, as in Tables 1 and 4. '*' denotes events which were statistically rejected but presented here based on tectonic consideration.

(2) The 'origin time' of an event is given by year, month, day, hour and minute.

(3) 'Notes': (I) Previously published solutions are cited (if available) by the reference, trend and the plunge of *P* and *T* axes; trend, plunge and rake of the fault (Fp) and the auxiliary (Ap) planes, or of the two nodal planes (Fp1 and Fp2). Ben-Menahem *et al.* (1976) solutions include plunge, trend and rake of the hanging block (e.g. Fp: 50/35, 125). (II) Data were mostly taken from ISS and ISC Bulletins. Additional sources were seismographic networks (e.g. ISN) or WWSSN stations (e.g. JER, HLW).

No	Origin time	Notes
1	194008161602	Event 8/40a. Based on too few stations with poor configuration on the stereogram. However, the solution is similar to the nearby mechanisms 2 and 15 and is therefore accepted.
2	194008161823	Event 8/40b. Based on too few stations with poor configuration, but accepted because it is similar to the nearby events 1 and 15.
3	194101200337	No comments.
4*	194509021154	Few stations and poor configuration. Similar to Ritsema (1974): Fp 1:45/130, 90; Fp 2:45/310, 90.
5	195104082138	Different solutions in: Canitez & Ucer (1967): Fp1: 71/118, 176; Fp2: 86/207, 19; and in Ben-Menahem *et al*. (1976): Fp: 50/35, 12.
6	195309100406	Different solution in: Wickens & Hodgeson (1967): Fp1: 86/174, 104; Fp2: 15/068, 15.
7	195509120609	Only the NW-dipping plane is constrained. Also appears in: Constantinescu *et al*. (1966): Fp1: 70/215, 157; Fp2: 69/116, 18; Canitez & Ucer (1967): Fp1: 57/45, 332; Fp2: 67/151, 36; Wickens & Hodgeson (1967): Fp1: 54/63, 141; Fp2: 60/307, 43; McKenzie (1972): Fp1: 52/153, 141; Fp2: 53/036, 45; Ritsema (1974): Fp1: 66/126, 027; Fp2: 65/048, 153; Ben-Menahem *et al*. (1976): Fp: 57/45, 332; Drakopoulos & Delibasis (1982): Fp1: 65/243, 129; Fp2: 46/126, 37
8	195603161932	Event 3/56a. Similar to mechanism 9.
9	195603161943	Event 3/56b. Poor solution, but similar to mechanism 8 (11 min earlier) and therefore is accepted.
10	195612181753	Different solution in: Wickens & Hodgeson (1967): Fp1: 35/265,161; Fp2: 80/160,56.
11*	195906131201	Based on a few stations with poor configuration. The mechanism is in accordance with the local tectonics and is therefore presented here.
12	196109150146	Similar solution in Buyukasikoglu (1980). Different solution in Canitez & Ucer (1967): Fp1: 13/050, 137; Fp2: 81/267, 80.
13	196309120818	Similar solution in Buyukasikoglu (1980).
14*	196501251218	Solution based on six first-motion readings only, but is compressional as expected.
15	196604081346	Based on a few stations with poor configuration. The solution is similar to mechanisms 1 and 2 and is therefore accepted.
16*	196704071707	Event 4/67a. Despite its high QF (high misfit), the mechanism is presented because of its similarity to the nearby event 17, which occurred 90 min later.
17*	196704071833	Event 4/67b presented despite its high QF (high misfit), because of its similarity to the nearby event 16 that occurred 90 min earlier.
18	196706151456	No comments.
19	196803261937	Different solution in Ben-Menahem *et al*. (1976): Fp: 70/290, 333.
20	196811061341	No comments.
21*	196903241154	Event 3/69a. High QF, but presented because of its similarity to the other nearby events. EIL.
22*	196903241250	Event 3/69b. Poor station distribution on the stereogram.
23*	196903270615	Event 3/69c. Based on few stations and high QF, but presented because of its tectonic significant. EIL.
24	196903310716	Event 3/69d. Dip direction of nodal planes is not constrained, but extension is always accepted. HLW, EIL. Similar solutions: McKenzie *et al*. (1970); Ben-Menahem & Aboodi (1971): Fp: 44/57, 309; Ap: 58/189, 239; Ben-Menahem *et al*. (1976): Fp: 45/45–60, 315; Huang & Solomon (1987): Fp: 40/18, −100; Jackson *et al*. (1988): Fp: 38/34, −85.
25	196903312144	Strike of fault plane is not constrained. HLW, EIL. 3/69e.
26	196904041218	Event 4/69a. EIL.
27	196904081031	Event 4/69b. Strike of the fault plane is not constrained. EIL.
28	196904231337	Event 4/69c. HLW, EIL.
29	196905100927	Strike of the fault plane is not constrained. EIL.
30*	196912300510	Poor station configuration, strike of the fault plane is not constrained, EIL.
31	197004280320	JER.
32*	197007011550	High QF and based on few stations, but in accordance with the local tectonics.
33	197010051453	Similar solution in Ben-Menahem *et al*. (1976): Fp: 64/150, 39; and in Chaimov *et al*. (1990).
34	197012192244	Data of the nearby 197012191215 event (not presented here) is similar to this solution.
35	197104162127	Among the set of multiple solutions found for this event, we preferred the one which is in accordance with the local tectonics. JER, EIL, AAE, QUE, SHI. Solution of Ben-Menahem *et al*.(1976): Fp: 64/261, 318.
36	197106290908	Additional reading from HLW.

37	197107082340	Event 7/71a. Strike of one nodal plane is not constrained. Different solution in Badawy (2001) P: 53/142, B: 32/358, T: 18/257.
38	197107112012	Event 7/71b. EIL. Similar to Ben-Menahem *et al*. (1976): Fp: 27/360, 90. Different solution in Badawy & Horvath (1999) P: 40/222, B: 50/40, T: 1/131.
39	197108170429	Aftershock of event 38 with similar mechanism.
40	197201120815	One nodal plane is not constrained. JER. Different solution in Badawy & Horvath (1999) P: 52/58, B: 38/245, T: 4/152.
41	197206280949	One nodal plane is not constrained. Similar to Jackson *et al*. (1988): Fp: 30/52, −80; and to Huang & Solomon (1987): Fp: 37/24, −89. Different solution in Badawy & Horvath(1999) P: 15/26, B: 70/247, T: 12/120.
42*	197404292005	High QF (high misfit). Different solution in Ben-Menahem *et al*. (1976): Fp: 65/47, 343. Different solution in Badawy & Horvath (1999) P: 45/264, B: 44/102, T: 9/3.
43*	197501010030	Event 1/75a. High QF. Among the set of multiple solutions we preferred the one that is in accordance with the local tectonics. EIL, JER.
44	197501282112	Event 1/75b. No comments.
45	197601121750	Additional reading from JER. 1/76a. Different solution in Badawy & Horvath (1999) P: 8/36, B: 50/136, T: 39/300.
46	197601122019	Similar to event 45. JER. 1/76b. Different solution in Badawy & Horvath (1999) P: 7/106, B: 41/10, T: 48/204.
47	197601262244	JER.
48	197802092110	JER.
49	197904042117	Event 4/79a. JER.
50	197904231301	Event 4/79b. Similar to Arieh *et al*. (1982): Fp: 60/290; Ap: 80/26. Different solution in Badawy & Horvath (1999) P: 8/133, B: 70/246, T: 18/41.
51*	197909201037	Solution is based on few stations with poor configuration but in accordance with the local tectonics. Similar to event 32.
52	198001021252	No comments.
53	198102190241	JER.
54	198106300759	JER.
xs 55	198108100521	No comments.
56*	198203231048	High QF and poor distribution of stations but in accordance with local tectonics. ISN.
57	198205200328	No comments.
58	198306030204	Event 6/83a. Additional data from ISN.
59	198306121200	Event 6/83b. High QF but clearly a thrust. Strike of nodal planes are not well constrained ISN. Different solution in Badawy & Horvath (1999) P: 5/24, B: 35/117, T: 55/287.
60	198309241640	ISN.
61	198311240014	No comments.
62*	198403292136	High QF but in accordance with the local tectonics. ISN. Similar to Badawy & Horvath (1999) P: 9/99, B: 80/260, T: 3/8.
63	198408240602	Similar to Hofstetter *et al*. (1989). Composite solution in Hofstetter *et al*. (1996): P: 2/87; T: 48/180; Fp: 60/55, 40; Ap: 56/302, 142. HRVD CMT (ISC): Fp1: 56/044, 0; Fp2: 90/134, 146. ISN. Similar to 19840828 (?) solution in Badawy & Horvath (1999) P: 3/238, B: 36/330, T: 54/143.
64	198411050115	The normal mechanism is in accordance with the local tectonics, although for hypocentre deeper than 8 km, a thrust solution is accepted. Different solution in: Hofstetter *et al*. (1989). Composite solution in Hofstetter *et al*.(1996): P: 73/34; T: 14/182; Fp: 60/190, −80; Ap: 31/350, −106. ISN.
65	198412181359	The *P*-axis is not well constrained.
66	198501250608	Similar to van Eck & Hofstetter (1990): P: 35/112; T: 54/299; Fp: 80/115, 93; Ap: 10/275, 70. ISN. Different solution in Badawy & Horvath (1999) P: 28/60, B: 62/344, T: 2/250.
67	198502281655	Additional data from ISN. Different solution in Badawy & Horvath (1999) P: 47/221, B: 43/32, T: 4/126.
68*	198512311942	Poor station coverage on the stereogram. One of the nodal planes is not constrained. ISN. Similar to Badawy & Horvath (1999) P: 62/17, B: 20/243, T: 18/146.
69*	198607071417	High QF but compressional as expected. ISN. Different solution in Badawy & Horvath (1999) P: 32/139, B: 58/327, T: 4/231.
70	198611262308	Similar to mechanisms 1, 2 and 14. ISN.
71	198701151119	Additional data from ISN. Similar to Badawy & Horvath (1999) P: 8/42, B: 23/135, T: 66/294.
72	198702180534	Additional data from ISN.
73	198704272041	Similar to van Eck & Hofstetter (1989): P: 10/324; T: 10/55; Fp: 90/100, −15; Ap: 75/100, −180. ISN.
74	198706160617	Only the westward-dipping plane is constrained.
75*	198709031239	High QF. ISN.
76	198710231632	Mechanism accepted at depth of 10 km. Shallower than 8 km or deeper than 15 km, a thrust is obtained. Similar to van Eck & Hofstetter (1990): P: 50/285; T: 36/79; Fp: 82/090, −76; Ap: 15/210, 150. ISN.
77*	198711090750	High QF. ISN.
78	198801300300	Similar to van Eck & Hofstetter (1990). ISN P: 18/119; T: 34/223; Fp: 80/085, 40; Ap: 50/166, 167.
79	198903310044	ISN. Different solution in Badawy & Horvath (1999) P: 7/182, B: 83/6, T: 0/272.
80	198909090516	ISN.
81*	199210121309	High QF but fits the tectonics. CSEM. Similar to Badawy & Horvath (1999) P: 52/138, B: 37/332, T: 6/237.